科技部補助專題研究計畫成果報告
期末報告

光敏感型兩性樹枝狀分子的合成、自組裝行為、與其在生醫上的應用

計 畫 類 別 ： 個別型計畫
計 畫 編 號 ： MOST 103-2113-M-040-003-
執 行 期 間 ： 103年08月01日至104年10月31日
執 行 單 位 ： 中山醫學大學醫學應用化學系(含碩士班)

計 畫 主 持 人： 朱智謙

計畫參與人員： 碩士班研究生-兼任助理人員：歐家禓
碩士班研究生-兼任助理人員：王珈宜
大專生-兼任助理人員：陳雅佩

處 理 方 式 ：
1.公開資訊：本計畫涉及專利或其他智慧財產權，2年後可公開查詢
2.「本研究」是否已有嚴重損及公共利益之發現：否
3.「本報告」是否建議提供政府單位施政參考：否

中 華 民 國 105 年 01 月 26 日

中 文 摘 要 ： 本計畫主要在開發具有光敏感特性的生物活性分子載體，透過光誘導裂解反應讓載體結構降解，進而釋放出所吸附的生物活性分子，以達到光控制釋放的目標。我們合成出可以透過光SN1機制而進行光解反應的香豆素酯衍生物，兩端分別接上疏水性的膽固醇與親水性的PAMAM樹枝狀分子，形成光敏感兩性分子載體。此樹枝狀分子可自我聚集形成類似微胞型態的偽樹枝狀高分子，接著利用外圍攜帶的多重胺基正電來吸附帶有多重負電的生物活性分子(如DNA)，形成穩定的樹枝狀複合體。最後可以利用照光來誘導的載體分子結構裂解，讓偽樹枝狀高分子瓦解後釋放出所攜帶的DNA分子，進入細胞後達到基因轉染的效果。我們主要利用數種光譜分析方法與Langmuir單分子層分析法來證實此兩性樹枝狀載體分子的自組裝、光誘導裂解與控制釋放的特性。

中 文 關 鍵 詞 ： 藥物釋放、光敏感、樹枝狀分子、香豆素、基因轉染

英 文 摘 要 ： This project aims to develop the photoresponsive materials as the synthetic vectors for carrying bioactive molecules. The carriers undergo a photolytic bond cleavage combined with structural degradation, and thus active photoinduced controlled release of the bioactive molecules toward target cells can be achieved. We have synthesized the amphiphilic dendrons composed of the coumarin ester-derived scaffold, which undergo a photo SN1 bond cleavage. Moreover, the bipolar nature makes the amphiphilic dendrons self-assembled to from a pseudodendrimer. The multiple positively charged NH2 groups at the peripheral is capable of interacting with polyanionic targets (e.g., DNA) to further yield the stable dendriplexes. Finally, UV-light stimulation can induce the dissociation of the dendriplexes based on the photocleavage of the coumarin ester building blocks, and therefore DNA can be released to enhance overall gene transfection efficiency. The self-assembly process and photoresponsive behavior were analyzed by several spectroscopic assay and by Langmuir monolayer technique.

英 文 關 鍵 詞 ： Drug delivery system, photoresponsive, dendrimers, coumarin, gene transfection

INTRODUCTION

Recently, using amphiphilic dendron architectures in which a hydrophobic group at the focal point encourages self-assembly of the resulting amphiphilic dendrons into large "pseudodendrimers".[1-6] This supramolecular strategy, allowing the combination of the characteristics of polymers and lipids, can give rise to a synergistic effect particularly in nucleic acids delivery. Recently, several research groups have demonstrated remarkable gene transfection *in vitro* and *in vivo* mediated by these amphiphilic dendrons.[7-10] For effective gene delivery, the synthetic carriers must overcome several extra and intracellular barriers.[11,12] Principally, using the "pseudodendrimers" as gene vector takes the advantage of dynamic and responsive association/dissociation towards nucleic acids, which favors not only the encapsulation of nucleic acids through the multivalent ligand array assembled by the dendrons but also rapid disassembly of these complexes under passive triggered condition (i.e., change in pH, ionic strength in target cells). Moreover, it has been suggested that complete dendron degradation would be required for effective nucleic acids decomplexation. However, the experimental and computer-aid simulation data have reported that structural degradation of the dendrons when bound to nucleic acids becomes ineffective on the transfection time scale even in lower pH associated with endosomes. This key problem makes the gene delivery a challenging task particularly for *in vivo* system.

The concept of phototriggers provide a useful strategy in the photo-controlled drug delivery system (DDS), because it permits rapid and accurate spatial and temporal control with external light stimulation.[13-18] The biological relevant bmaterials containing a photocaged building block can undergo efficient photolysis through active phototriggers, thus leading to the structural degradation combined with the releasing of bioactive payloads. One of the most well-known light-absorbing photocages is the cormarin family, which allows one- or two-photon-regulated drug release.[19-24] Because the coumarin derivatives undergo a photosolvolysis via a photo S_N1 mechanism, the microenvironment for achieving effective bond cleavage requires access to a nucleophile in a protic media (typically water).[25,26] Besides, the intrinsic fluorescence nature of the coumarin ring makes these photocages a robust fluorescence probe for simultaneously imaging biodistribution of the DDS in living tissues.[23]

In this study, we aim to develop the amphiphilic dendritic scaffolds with a photocage for creating photoresponsive pseudodendrimer that can achieve controlled release under active light trigger. The amphiphilic structure composed of a hydrophilic poly(amido amine) (PAMAM) dendron and a lipophilic cholesterol molecule combines the advantageous gene delivery feature of both lipid and polymer vector. As shown in Figure 1, the amphiphilic counterpart is further interconnected by a photolabile coumarin ester, allowing the photo-induced degradation of the amphiphilic structure. The arrow indicates an electrophilic allylic carbon, and the C-O bond can be readily cleaved in the

presence of nucleophiles under light illumination. Consequently, this strategy provides an active route to accelerate the nucleic acids releasing and to enhance the efficiency gene transfection. Moreover, to study insight into the self-assembly process of the amphiphiles and their photoresponsive behavior, Langmuir techniques was introduced to investigate the interfacial phenomenon at the air-water interface. We also believed that thus-formed Langmuir monolayers are more fluid and provide a more realistic model for studying DNA binding and phototriggered releasing.

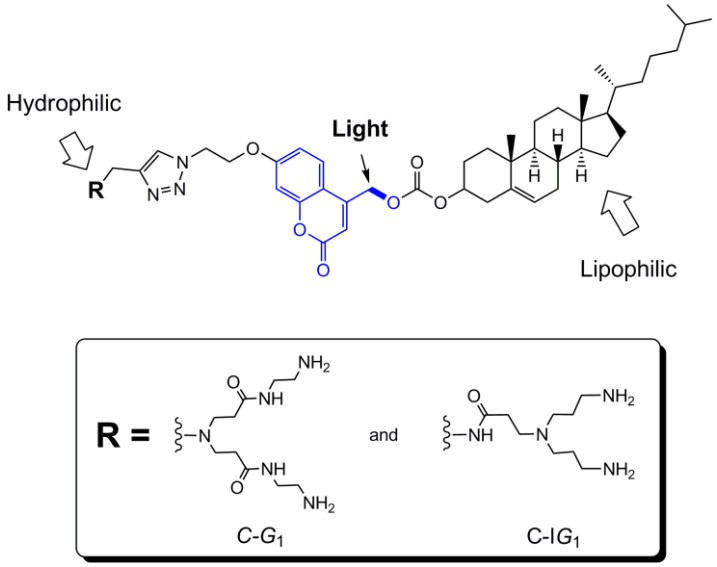

Figure 1. Coumarin-derived amphiphilic dendrons.

RESULTS AND DISCUSSION

As shown in Scheme 1, the azide-functionalized cholesterol and coumarin conjugate ***1*** was synthesized from a commercial available 7-hydroxy-4-methylcoumarin in 4 steps. On the basis of our design, the cholesterol not only act as the lipophilic head but also assist cellular uptake by enhancing the penetration across a cell membrane. The interconnecting coumarin-derived carbonate ester is highly sensitive to UV light and the photolabile C-O bond (marked in bold) is readily cleaved to recover the compound ***2*** and a free cholesterol molecule.

The time-dependent photolytic reaction of compound ***1*** was monitored by UV-Vis absorption and fluorescence spectra. The maximum absorption and emission wavelength of ***1*** were found to be 320 and 390 nm, respectively. As shown in Figure 2a, the absorbance at 320 nm only slightly decreases as a sample solution was exposed to 365 nm light emitting diode (LED); however, the fluorescence intensity at 390 nm gradually increases as the irradiation time is increased (Figure 2b). The fluorescence enhancement is attributed to the S_N1-like photocleavage of the coumarin ester to yield a free cholesterol molecule. Moreover, HPLC analysis shows the depletion of the retention peak of

compound ***1*** (Figure 2c), and GC-MS analysis shows the characteristic peak of cholesterol at 10.2 min after light exposure (Figure 2d). The results all suggest a successful photolytic reaction and structural degradation of the coumarin derivative.

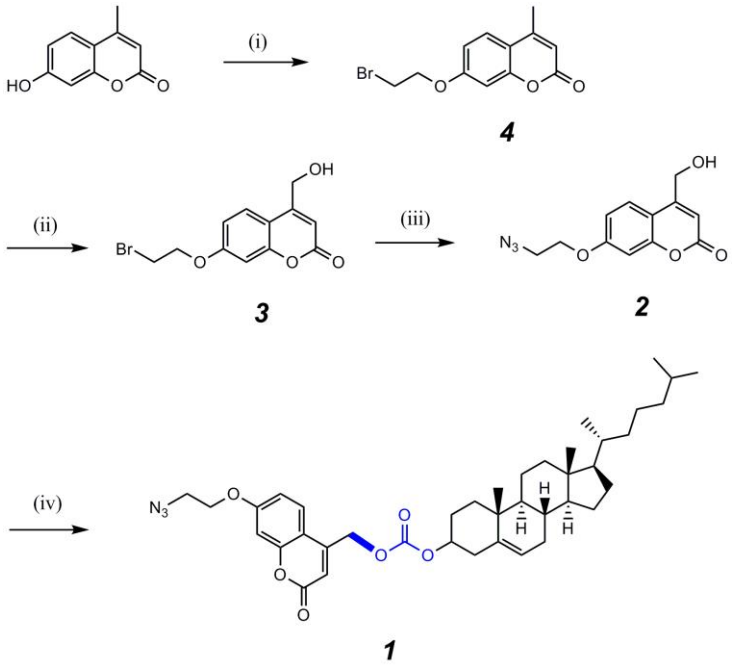

Scheme 1. Synthetic route for compound ***1***.

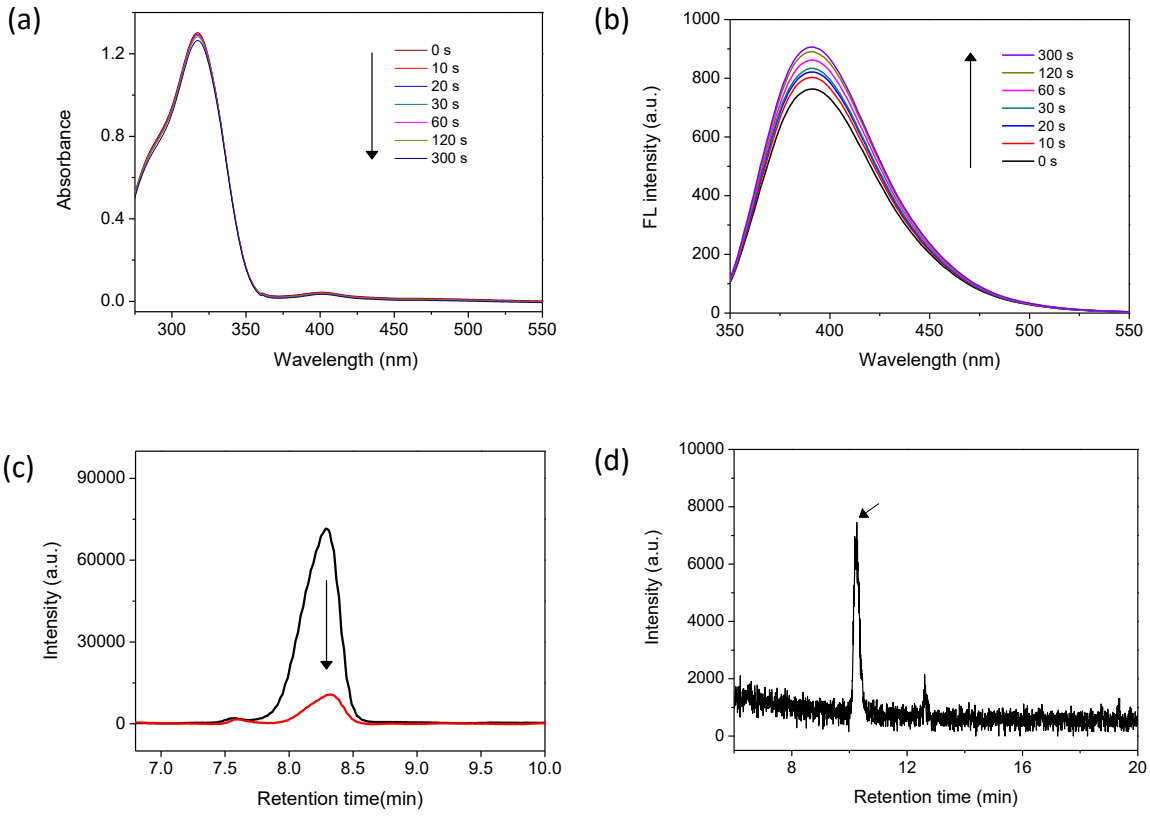

Figure 2. (a) UV-Vis absorption analysis. (b) Fluorescence analysis. (c) HPLC analysis. (d) GC-MS analysis.

The copper(I)-catalyzed azide-alkyne cycloaddition (CuAAC) between alknyl-functionalized PAMAM dendrons and compound ***1*** affords the amphiphilic dendrons, namely C-G_1 and C-IG_1 (Figure 1). Notably, both dendrons have two primary amine terminals but possess inverse tertiary amine branch to amide linkage. The two amphiphilic dendrons were well-characterized by NMR and MS analysis. The click conjugation was confirmed according to the appearance of the triazole proton resonances, and the observed mass values were consistent with the calculated values of the protonated adducts of C-G_1 and C-IG_1.

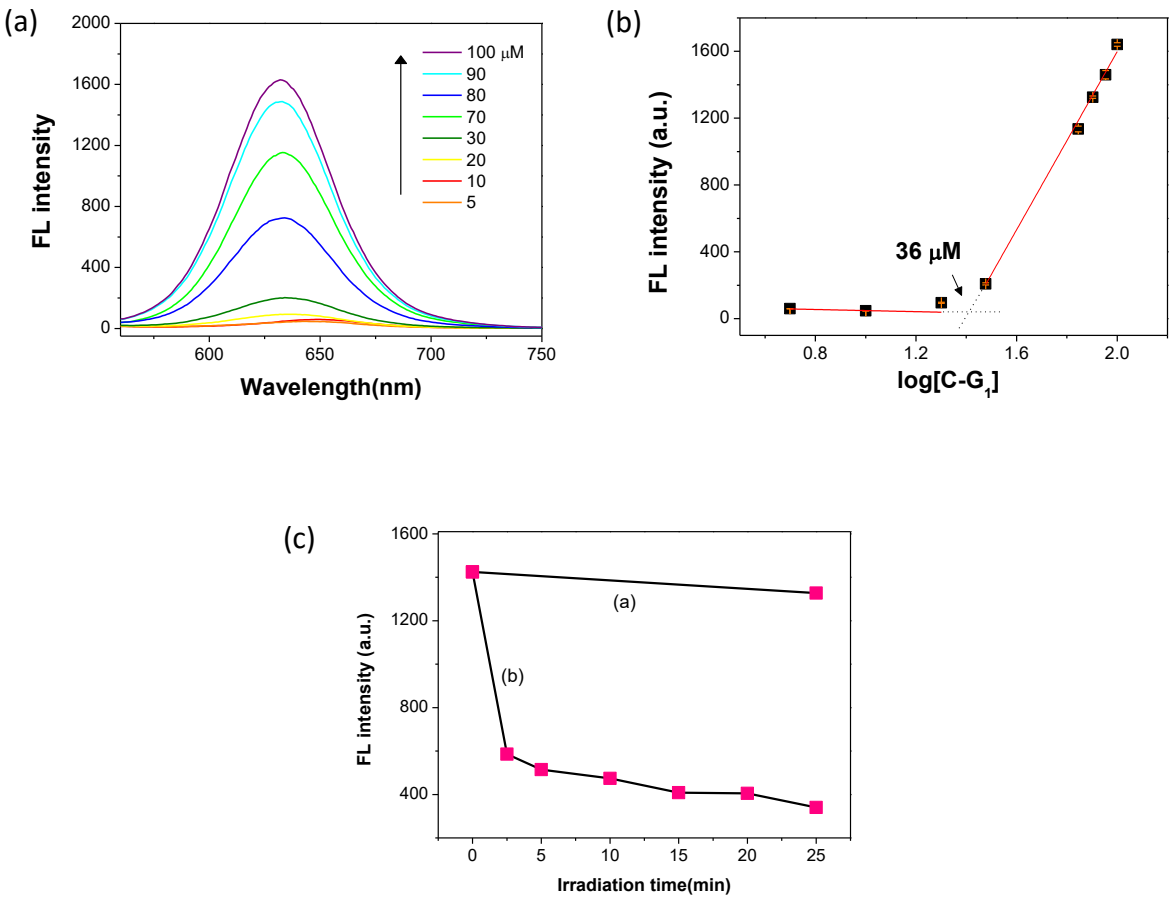

Figure 3. (a) Nile-red solubilization fluorescence analysis. (b) Critical aggregation concentration of C-G_1. (c) The change in fluorescence intensity after 365-nm light irradiation.

Because of the amphiphilic structure composed of a hydrophilic PAMAM Dendron and a lipophilic cholesterol, C-G_1 and C-IG_1 could assemble into Percec-type pseudodendrimes with a micelle-like structure in an aqueous media. This self-assembly process was confirmed using a Nile-red solubilization fluorescence assay, in which hydrophilic Nile-red dyes are used to observe the formation of a hydrophobic domain of the cholesterols within an assembled nanostructure. Accordingly, Nile-red is solubilized and then emits appreciate orange-red fluorescence (Figure 3a). Moreover, Figure 3b shows that the self-assembly was observed with discontinuity in the fluorescence intensity of Nile red at 635 nm plotted against increasing dendron concentration at the

critical aggregation concentration (CAC). The CAC for C-G_1 and C-IG_1 could be identified as approximately 36 and 39 μM, respectively, which is much lower than that for a coumarin-derived surfactant. This result suggests the amphiphilic dendrons possess more effective self-assembly process.

The photocleavable building block of coumarin ester makes the self-aggregated micelles readily dissociated under UV light irradiation. This deformation can be also analyzed by the Nile red probes encapsulated within the micelles. In contrast to the controlled experiment that the solution stored in dark only exhibits slight decrease in fluorescence intensity, light irradiation is capable of causing drastically fluorescence decrement until reaching a plateau (Figure 3c). This result suggests that the micelles are stable until active light stimulation to degrade these self-assemble structures.

To study insight into the self-assembly of two amphiphiles and their photoresponsive property, Langmuir technique was introduced to investigate the interfacial phenomenon at the air-water interface. As shown in Figure 4a, the π-A isotherms shows that both C-G_1 and C-IG_1 possess significant compressibility and end up forming homogeneous Langmuir monolayers upon compression until the surface pressure of collapse approximately equals to 50 mN/m. This result evidently suggests that the amphiphilic structure favors the molecular assembly at air-water interface. Notably, the final molecular area in a compressed film for C-G_1, after extrapolation to zero surface pressure, is slightly larger than that for C-IG_1. This result implied that the hydrophilic dendritic cone of a single C-G_1 occupies more area at the interface than that of C-IG_1, and therefore C-G_1 exhibits lower CAC value.

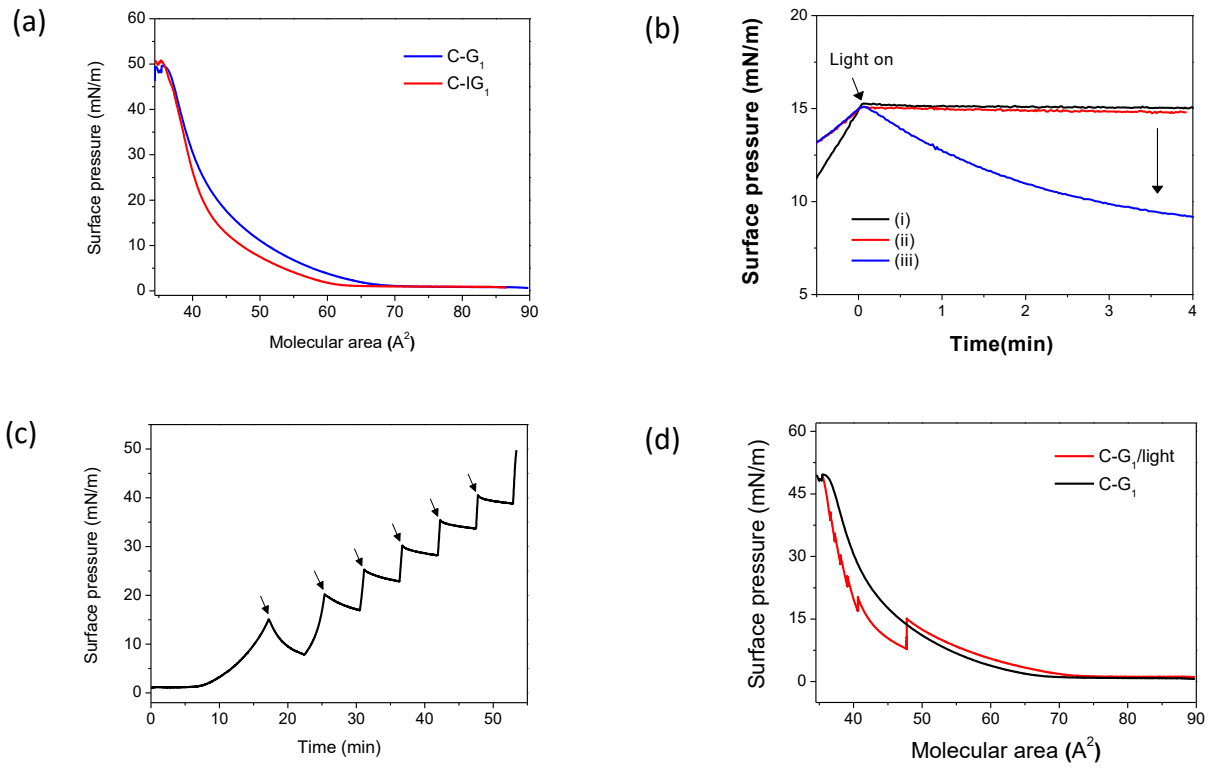

Figure 4. Langmuir analysis for the monolayer of C-G_1.

After confirming both amphiphilic dendrons are capable of processing molecular assembly at the interface, we attempted to examine the photoresponisve behavior of the assembled structures. Firstly, a monolayer at a certain surface pressure (~ 15 mN/m) and molecular area by keeping the barriers constant was prepared, and then the equilibrium was continuously disturbed by UV light irradiation. Figure 4b shows the correlation of elapsed time (t) with surface pressure recorded exactly after photo stimulation was activated (t = 0). The surface pressure of the monolayer composed of C-G_1 gradually decreases as the light was turned on (blue line); in contrast, this monolayer is quite stable under dark (red line). Moreover, the monolayer of stearic acids, being unresponsive to 365-nm UV light, also remains unchanged under light exposure (black line). Taking the three data into account, Langmuir technique discloses a consistent message that the assembled structure composed of the coumarin-based amphiphilic dendron is highly sensitive to UV light. The bond cleavage between the coumarin ester and cholesterol at the interface results in the collapse of the monolayer under light stimulation.

However, the monolayer at the interface is only partially collapsed upon light exposure, because it can be reconstructed by continuous compression in the absence of light. As shown in Figure 4c, the surface pressure was initially decreased under light excitation (black arrows) but can be increased again by barrier compression as the light was turned off. The photoinduced collapse and reconstruction of the monolayer can be alternatively manipulated until reaching the maximum pressure of approximately 50 mN/m. In addition, the isotherm shows a smaller final molecular area (Figure 4d), which suggests the concentration of the amphiphilic dendrons significantly drops because they are gradually destroyed during every period of light exposure. The Langmuir analysis concluded that photo stimulation strategy did provide accurate spatial and temporal control over the integrity of the self-assembled system.

Once the coumarin-based amphiphilic dendrons self-aggregates into assembled pseudodendrimers with positively charged peripherals, it can effectively interact with polyanionic bioactive targets suchlike DNA to form dendriplexes through electrostatic interaction. The binding and photoinduced releasing were then analyzed by ethidium bromide (EtBr) displacement assay. This assay method involves using the competition between the DNA binder and EtBr to determine the concentration at which the DNA binder takes effect. This concentration can be expressed as a charge excess (CE_{50}) value, which reflects the concentration of the DNA binder required for half of the EtBr to be displaced from binding to DNA. This value is also the equivalent of a minimum nitrogen-to-phosphorus (N/P) ratio that is usually used to determine the amount of amine-based binding motifs required for effective DNA condensation through electrostatic interactions between the amine and phosphate groups.

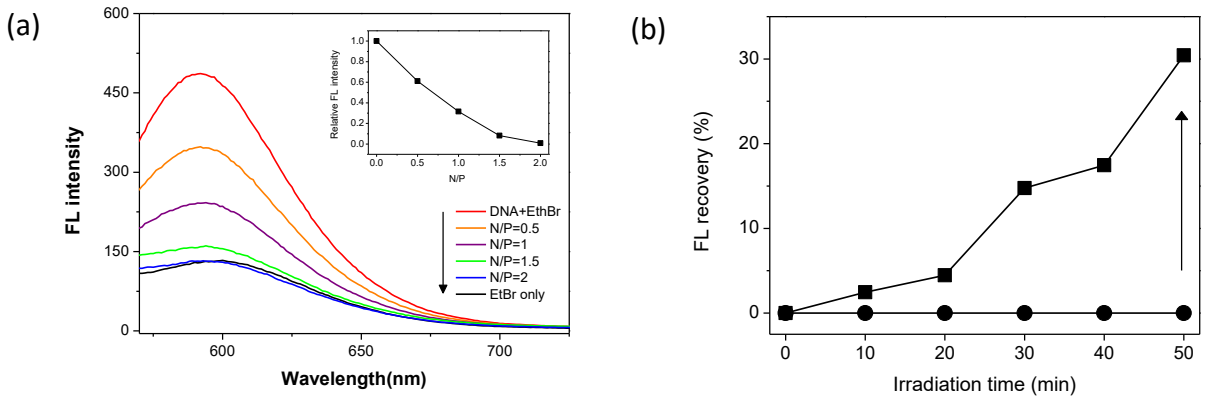

Figure 5. (a) Fluorescence titration data of ethidium bromide displacement assay. (b) The recovery of the emission of ethidium bromide after 365-nm light irradiation.

Figure 5a shows the fluorescence titration experiment by increasing the concentration of C-G_1 at constant amounts of DNA (0.5 μg) and EtBr (0.7 μg). Initially, EtBr undergoes a large increase in fluorescence intensity upon intercalation with stacks of nucleic acid base pairs. However, the fluorescence quenching of the EtBr/DNA complexes occurs in the presence of amine-based vectors, which is due to the competitive displacement of EtBr by those vectors. The emission intensity at 590 nm gradually decreases as the N/P values are increased, suggesting the dendriplex formation by increasing the concentration of C-G_1. The CE_{50} calculated from the titration data is found to be approximately less than 1, which is consistent with previous study using the cholesteryl-derived amphiphilic PAMAM dendron as DNA vectors. Moreover, we reasoned that as the vectors degraded under UV light exposure, the DNA should be released and the EtBr is reintercalated into the double helix, thus reactivating its fluorescence. Accordingly, Figure 5b shows the fluorescence increment from the minimum intensity of the DNA/C-G_1 complexes at N/P =2 after LED light excitation. In sharp contrast, the fluorescence intensity remains static when the complex solution was only kept in dark. This result confirms that the photolytic reaction of the vectors did induce the decomplexation accompanied with DNA escape under an active phototriggered route.

After light exposure for 50 min, the fluorescence intensity was partially recovered to approximately 30% of the original magnitude for the emission of DNA/EtBr complex in the absence of the dendritic vectors (N/P = 0). This result implies that only 30% of DNA is released from the dendriplexes upon light excitation. We assume that assembled dendrons is more resistant to the photoinduced disruption than a single dendron did. The Langmuir analysis also reveals that the assembled structure will soon be recovered under external compression after a partial collapse. It is believed that these electrostatic complexes are quite tough against the environmental fluctuation. Although UV light is insufficient to induce “complete” dissociation of the DNA complexes using coumarin-derived amphiphilic dendron as the vector, it did assist the release of the nucleic acids.

Conclusions

In summary, we successfully synthesized photoresponsive amphiphilic PAMAM dendrons bearing photolabile coumarin ester building blocks as DNA carriers. Both amphiphilic dendrons (C-G_1 and C-IG_1) exhibit self-assembly behavior in the formation of micelle-like pseudodendrimers in an aqueous solution, which was elegantly confirmed by spectroscopic and Langmuir isotherm analysis. On the basis of the bipolar functionality, C-G_1 and C-IG_1 also demonstrate substantial binding affinity with cyclic DNA at low N/P values. Most critically, thus-formed DNA complexes are readily dissociated under UV light irradiation because the coumarin ester group in the dendritic structure undergoes efficient photolytic cleavage, causing effective dendron degradation accompanied by DNA release.

Acknowledgments

We would like to thank Chung Shan Medical University and Ministry of Science and Technology (MOST) of Taiwan, for financially supporting this research (MOST 103-2113-M-040-003). NMR analysis was performed in the Instrument Center of Chung Shan Medical University, which is supported by Ministry of Education and Chung Shan Medical University.

References

(1) Posocco, P.; Pricl, S.; Jones, S.; Barnard, A.; Smith, D. K. *Chem. Sci.* **2010**, *1*, 393.

(2) Jones, S. P.; Gabrielson, N. P.; Wong, C.-H.; Chow, H.-F.; Pack, D. W.; Posocco, P.; Fermeglia, M.; Pricl, S.; Smith, D. K. *Mol. Pharm.* **2011**, *8*, 416.

(3) Welsh, D. J.; Smith, D. K. *Org. Biomol. Chem.* **2011**, *9*, 4795.

(4) Barnard, A.; Smith, D. K. *Angew. Chem. Int. Ed.* **2012**, *51*, 6572.

(5) Barnard, A.; Posocco, P.; Fermeglia, M.; Tschiche, A.; Calderon, M.; Pricl, S.; Smith, D. K. *Org. Biomol. Chem.* **2014**, *12*, 446.

(6) Thota, B. N. S.; Berlepsch, H. v.; Bottcher, C.; Haag, R. *Chem. Commun.* **2015**, *51*, 8648.

(7) Kono, K.; Ikeda, R.; Tsukamoto, K.; Yuba, E.; Kojima, C.; Harada, A. *Bioconjugate Chem.* **2012**, *23*, 871.

(8) Yu, T.; Liu, X.; Bolcato-Bellemin, A.-L.; Wang, Y.; Liu, C.; Erbacher, P.; Qu, F.; Rocchi, P.; Behr, J.-P.; Peng, L. *Angew. Chem. Int. Ed.* **2012**, *51*, 8478.

(9) Yuba, E.; Nakajima, Y.; Tsukamoto, K.; Iwashita, S.; Kojima, C.; Harada, A.; Kono, K. *J. Controlled Release* **2012**, *160*, 552.

(10) Liu, X.; Liu, C.; Zhou, J.; Chen, C.; Qu, F.; Rossi, J. J.; Rocchi, P.; Peng, L. *Nanoscale* **2015**, *7*, 3867.

(11) Barnard, A.; Posocco, P.; Pricl, S.; Calderon, M.; Haag, R.; Hwang, M. E.; Shum, V. W. T.; Pack, D. W.; Smith, D. K. *J. Am. Chem. Soc.* **2011**, *133*, 20288.

(12) Draghici, B.; Ilies, M. A. *J. Med. Chem.* **2015**, *58*, 4091.

(13) Lee, R.-S.; Wang, S.-W.; Li, Y.-C.; Fang, J.-Y. *RSC Adv.* **2015**, *5*, 497.
(14) Jiang, Z.; Li, H.; You, Y.; Wu, X.; Shao, S.; Gu, Q. *J. Biomed. Mater. Res. A* **2015**, *103*, 65.
(15) Shah, S.; Sasmal, P. K.; Lee, K.-B. *J. Mater. Chem. B* **2014**, *2*, 7685.
(16) Jin, Q.; Wang, Y.; Cai, T.; Wang, H.; Ji, J. *Polymer* **2014**, *55*, 4641.
(17) Huang, Q.; Liu, T.; Bao, C.; Lin, Q.; Ma, M.; Zhu, L. *J. Mater. Chem. B* **2014**, *2*, 3333.
(18) Fedoryshin, L. L.; Tavares, A. J.; Petryayeva, E.; Doughan, S.; Krull, U. J. *ACS Appl. Mater. Interfaces* **2014**, *6*, 13600.
(19) Lin, Q.; Bao, C.; Cheng, S.; Yang, Y.; Ji, W.; Zhu, L. *J. Am. Chem. Soc.* **2012**, *134*, 5052.
(20) Lin, Q.; Bao, C.; Fan, G.; Cheng, S.; Liu, H.; Liu, Z.; Zhu, L. *J. Mater. Chem.* **2012**, *22*, 6680.
(21) Lin, Q.; Bao, C.; Yang, Y.; Liang, Q.; Zhang, D.; Cheng, S.; Zhu, L. *Adv. Mater.* **2013**, *25*, 1981.
(22) Zheng, K.; Lin, W.; Tan, L.; Chen, H.; Cui, H. *Chem. Sci.* **2014**, *5*, 3439.
(23) Barman, S.; Mukhopadhyay, S. K.; Gangopadhyay, M.; Biswas, S.; Dey, S.; Singh, N. D. P. *J. Mater. Chem. B* **2015**, *3*, 3490.
(24) Gangopadhyay, M.; Mukhopadhyay, S. K.; Karthik, S.; Barman, S.; Pradeep Singh, N. D. *MedChemComm* **2015**, *6*, 769.
(25) Furuta, T.; Wang, S. S. H.; Dantzker, J. L.; Dore, T. M.; Bybee, W. J.; Callaway, E. M.; Denk, W.; Tsien, R. Y. *Proceedings of the National Academy of Sciences of the United States of America* **1999**, *96*, 1193.
(26) Eckardt, T.; Hagen, V.; Schade, B.; Schmidt, R.; Schweitzer, C.; Bendig, J. *J. Org. Chem.* **2002**, *67*, 703.

NJC

PAPER

Photodegradable self-assembling PAMAM dendrons for gene delivery involving dendriplex formation and phototriggered circular DNA release†

Yu-Sen Lai,[a] Chai-Lin Kao,[b] Ya-Pei Chen,[a] Chia-Chia Fang,[a] Chao-Chin Hu[a] and Chih-Chien Chu*[ac]

Cite this: DOI: 10.1039/c5nj03173g

Received (in Montpellier, France) 11th November 2015,
Accepted 14th January 2016

DOI: 10.1039/c5nj03173g

www.rsc.org/njc

For effective gene delivery, structural degradation of synthetic carriers is crucial to the release of nucleic acids on the transfection time scale. In this study, we have synthesized the amphiphilic dendritic scaffolds with a photolabile *o*-nitrobenzyl (*o*-NB) group that can enable the structural decomposition and controlled release of nucleic acids under active light stimulation. The amphiphilic counterpart composed of a lipophilic cholesterol and a hydrophilic poly(amido amine) (PAMAM) dendron allows the self-assembly into a core–shell-like pseudodendrimer above the critical aggregation concentration (CAC) of approximately 20 μM. On the basis of electrostatic interaction, the polycationic pseudodendrimers are capable of forming stable complexes with polyanionic cyclic reporter genes under low charge excess values, suggesting substantial binding affinity of the dendron assembly toward circular DNA. Because the *o*-NB group in the dendritic structure undergoes efficient photolytic cleavage, an *in vitro* test shows that thus-formed "dendriplexes" are readily dissociated under 365 nm light irradiation, causing effective dendron degradation accompanied by DNA release. This photochemical strategy provides an opportunity to control gene binding and release in a spatiotemporal manner.

Introduction

Dendrimers based on tailor-made surface functional groups and multivalent properties have been suggested as promising nanoscale synthetic carriers for delivering bioactive materials into target cells. An alternative to the processes required to prepare giant dendrimers with a well-defined hyperbranched structure, which are tedious and time-consuming, is using small amphiphilic dendron architectures in which a hydrophobic group at the focal point encourages the self-assembly of the resulting amphiphilic dendrons into large "pseudodendrimers."[1–6] This supramolecular strategy, which enables combining the polymer and lipid characteristics, can cause a synergistic effect, particularly in nucleic acid delivery. Recently, several studies have demonstrated remarkable DNA and small interfering RNA (siRNA) transfection *in vitro* and *in vivo* mediated by these amphiphilic dendrons.[7–10]

For effective gene delivery, synthetic carriers must overcome several extracellular and intracellular barriers including (1) nucleic acid complexation and protection, (2) cell membrane penetration, (3) endosomal escape, and (4) nucleic acid release for gene expression or knockdown.[11,12] Principally, using the pseudodendrimers as gene vectors enables taking advantage of dynamic and responsive association and dissociation toward nucleic acids, which favors the encapsulation of nucleic acids through the multivalent ligand array assembled by the dendrons and rapid disassembly of these complexes under external stimuli (*e.g.*, change in pH or ionic strength).[13,14] To achieve the controlled release of nucleic acid after it enters the cells, complete dendron degradation has been suggested as mandatory for effective nucleic acid decomplexation. However, experimental and computer-aided simulation data have revealed that the structural degradation of the dendrons when bound to nucleic acids becomes ineffective on the transfection time scale, even at the lower pH associated with endosomes.[11] This key problem associated with barrier 4 on the transfection pathway makes gene delivery a challenging task, particularly for *in vivo* gene transfection.

[a] *Department of Medical Applied Chemistry, Chung Shan Medical University, Taichung 40201, Taiwan. E-mail: jrchu@csmu.edu.tw*
[b] *Department of Medical and Applied Chemistry, Kaohsiung Medical University, Kaohsiung 80708, Taiwan*
[c] *Department of Medical Education, Chung Shan Medical University Hospital, Taichung 40201, Taiwan*

† Electronic supplementary information (ESI) available: Materials synthesis, NMR characterization, mass spectrometric data, particle size and zeta potential analysis. See DOI: 10.1039/c5nj03173g

Recently, the concept of phototriggers has provided a useful strategy in photocontrolled drug delivery systems (PDDSs) because it enables rapid and accurate control over specific sites and times with external light stimulation.[15–20] Biologically relevant materials containing a photolabile building block can undergo efficient photolysis through active phototriggers, thus causing structural degradation and the release of biological targets. Among the numerous photolabile groups that have been studied, *o*-nitrobenzyl (*o*-NB) alcohol derivatives have aroused much attention in the PDDS field.[21–24] *o*-NB alcohol derivatives that undergo efficient photoisomerization are readily cleaved upon irradiation with UV light (approximately 300–350 nm) and then release a free carboxylic acid (COOH) and *o*-nitrosobenzaldehyde.[25] Because the *o*-NB group is highly sensitive to UV light, this photocleavage reaction can be induced within minutes, even when using a low-intensity light source. Moreover, simple chemical modifications to an aromatic ring enable the tuning of the absorption profiles of the *o*-NB group slightly. For example, an electron-donating substituent (*e.g.*, OCH_3) functionalized at the *para* position of the NO_2 group can bathochromically shift the photocleavage wavelength to within the 350–400 nm range.

In this paper, we present amphiphilic dendritic scaffolds with a photolabile building block for creating photoresponsive pseudodendrimers that can enable the controlled release of nucleic acids under active light triggering. Generally, the amphiphilic structure composed of a hydrophilic poly(amido amine) (PAMAM) dendron and a lipophilic cholesterol molecule combines the advantageous gene delivery feature of lipid and polymer vectors. Furthermore, to overcome barrier 4, the cholesterol and dendron are interconnected by a photolabile *o*-NB group, enabling photoinduced degradation of the amphiphilic structure. Consequently, this strategy provides a remotely triggered route for accelerating nucleic acid release and enhancing gene transfection efficiency.[26] Aside from classical PAMAM dendrons, the novel dendron analogue that has inverse amide linkage to the amine branch are introduced for constructing the amphiphilic structures (Fig. 1).[27]

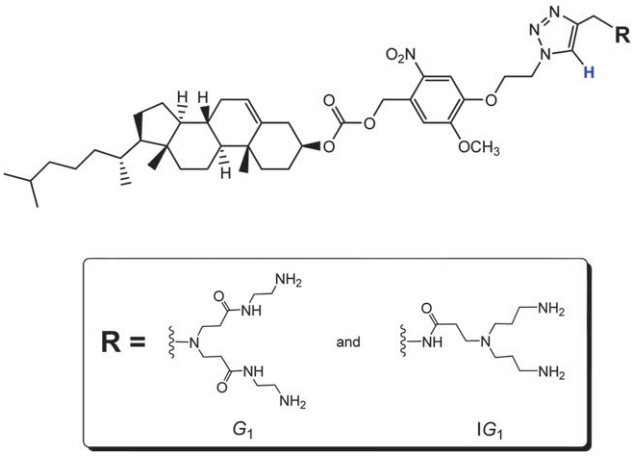

Fig. 1 The *o*-nitrobenzyl (*o*-NB)-containing amphiphilic PAMAM dendrons. The H denotes the characteristic triazole protons of the click clusters.

Results and discussion

Dendron synthesis and characterization

Fig. 1 shows the classical PAMAM dendron and its analogue, namely $\mathbf{G_1}$ and $\mathbf{IG_1}$ respectively. $\mathbf{G_1}$ dendron was synthesized through consecutive 1,4-Michael addition and amidation, with propargyl amine used as the starting material.[28] Moreover, $\mathbf{IG_1}$ dendron with a COOH focal point was prepared using the synthetic method developed by Huang *et al.*[27] Carbodiimide-promoted amidation of $\mathbf{IG_1}$ with propargyl amine yields the final propargyl-functionalized inverse dendrons. All amino groups of both dendrons were protected by the *tert*-butyloxycarbonyl (Boc) groups to prevent unwanted complexation of copper catalysts with NH_2 groups during the click reaction.

As shown in Scheme 1, the *o*-NB alcohol derivative **1** was synthesized from commercially available vanillic aldehyde by following a modified procedure.[29] A nucleophilic substitution reaction at the phenolic proton yields compound **2**; following this an azide substitution yields compound **3**. Subsequently, a simple esterification of **3** with cholesteryl chloroformate yields precursor **4** with a carbonate linkage between the cholesterol and the *o*-NB group. The terminal azide group enables "click" conjugation with propargyl-functionalized classical and inverse PAMAM dendrons through [3+2] copper-catalyzed azide–alkyne click reaction (CuAAC) protocols.[28] Finally, acid-promoted hydrolysis of the click products to remove the Boc protection yields the desired amphiphilic dendrons, namely $\mathbf{Chol\text{-}G_1}$ and $\mathbf{Chol\text{-}IG_1}$, with photolabile *o*-NB building blocks.

Because the amphiphilic dendrons could exist in the form of giant aggregates rather than a single molecule in water or organic solvents, interpreting NMR spectra becomes a difficult task based on these complex resonance patterns of $\mathbf{Chol\text{-}G_1}$ and $\mathbf{Chol\text{-}IG_1}$ (see ESI,† Fig. S3). Fortunately, successful click conjugation was readily confirmed according to the appearance of the triazole proton resonances at δ = 8.42 and 8.04 ppm, which correspond to the characteristic protons in the triazole linkages of $\mathbf{Chol\text{-}G_1}$ and $\mathbf{Chol\text{-}IG_1}$, respectively (Fig. 1). Moreover, the 1 : 1

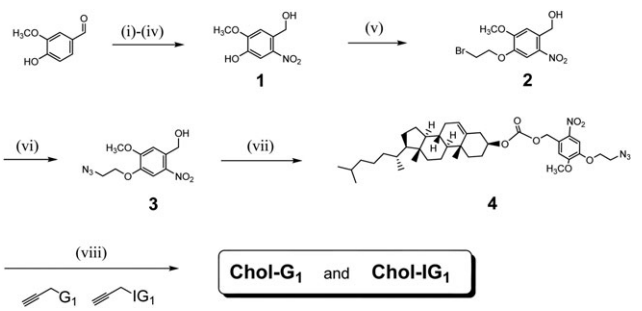

Scheme 1 Synthetic conditions: (i) benzyl chloride, K_2CO_3, DMSO, 90 °C; (ii) 65% HNO_3, CH_3COOH, ice bath to 25 °C; (iii) CF_3COOH, 25 °C; (iv) $NaBH_4$, EtOH, 25 °C; (v) 1,2-diboromoethane, K_2CO_3, 18-crown-6, THF, 40 °C; (vi) NaN_3, DMF, 90 °C; (vii) cholesteryl chloroformate, pyridine, THF, 40 °C; (viii) CuBr, THF, and then CF_3COOH, CH_2Cl_2, 25 °C.

integration ratio between the triazole proton and aromatic proton on the *o*-NB ring suggests effective CuAAC reaction of azide-terminated compound **4** with propargyl-functionalized $\mathbf{G_1}$ or $\mathbf{IG_1}$ dendron. More evidently, the absolute molecular weights for the amphiphilic dendrons were analyzed by performing MALDI-TOF-MS, with α-cyano-4-hydroxycinnamic acid used as a supporting matrix. The observed mass values were consistent with the calculated values of the protonated adducts of **Chol-$\mathbf{G_1}$** and **Chol-$\mathbf{IG_1}$** at 964.6 and 921.4 Da, respectively.

Self-assembly and photo-induced disassembly of dendrons

Because of the amphiphilic nature of a structure composed of a hydrophilic PAMAM dendron and a lipophilic cholesterol, **Chol-$\mathbf{G_1}$** and **Chol-$\mathbf{IG_1}$** assemble into Percec-type pseudodendrimers in an aqueous solution.[30] The structure of the pseudodendrimers is based on a core–shell-like micelle, in which the cholesterol aggregates are sheltered with PAMAM dendrons in aqueous media. The hydrophilic and lipophilic balance dominates the size, integrity, and morphology of the micelle-like pseudodendrimers. This self-assembly process was further confirmed using a Nile-red solubilization fluorescence assay, in which hydrophobic Nile-red dyes are used to observe the formation of a hydrophobic domain within an assembled nanostructure.[3,31] Nile red is solubilized and emits appreciable orange-red fluorescence only when the dendron itself self-assembles into a micelle with a hydrophobic domain. Fig. 2a and b shows that the self-assembly process was observed for **Chol-$\mathbf{G_1}$** and **Chol-$\mathbf{IG_1}$**, with discontinuity in the fluorescence intensity of Nile red at 635 nm plotted against increasing dendron concentration at the critical aggregation concentration (CAC). These results confirm that self-assembly occurs above the CAC. Using the Nile-red assay, the CAC for **Chol-$\mathbf{G_1}$** and **Chol-$\mathbf{IG_1}$** in phosphate buffer solution could be identified as approximately 20 μM, which is comparable to the CAC of cholesterol-based spermine dendrons.[1] In addition, we used dynamic light scattering (DLS) methods and assumed a spherical aggregation to further analyze the particle size of the self-assembled aggregates. The dimensions of **Chol-$\mathbf{G_1}$** and **Chol-$\mathbf{IG_1}$** aggregates formed in a phosphate buffer solution were approximately 114 ± 0.9 and 130 ± 1.4 nm, respectively.

Because the photocaged *o*-NB derivatives exhibit moderate absorption in the UV region, we examined the photoinduced degradation of the amphiphilic dendrons by using ultraviolet-visible (UV-Vis) spectroscopic analysis. The photocleavage reaction can be conducted under UV light; therefore, both dendron solutions were exposed to a 365 nm light-emitting diode (LED) at fixed time intervals (10, 20, and 30 min). Fig. 3a and b illustrates the apparent changes in the absorption profiles of the **Chol-$\mathbf{G_1}$** and **Chol-$\mathbf{IG_1}$** solutions, respectively, upon UV light exposure. Furthermore, the **Chol-$\mathbf{IG_1}$** dendron possesses observable red-shifted absorption bands in the UV region (300–400 nm). This result clearly suggests the structural decomposition of the *o*-NB moiety from the original *o*-nitrobenzyl carbonate into *o*-nitrosobenzaldehyde after UV light irradiation.[32] Moreover, for both solutions, the appearance of a detectable

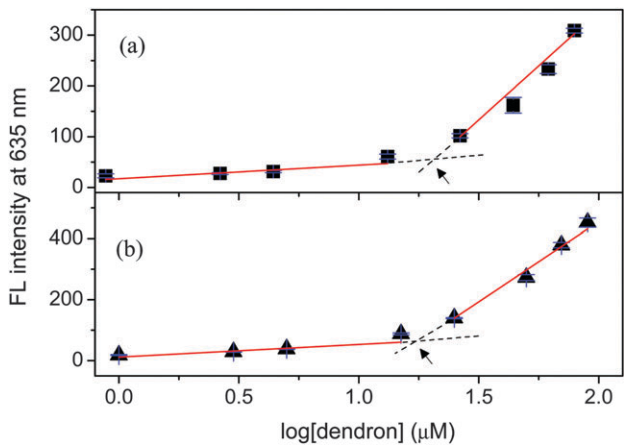

Fig. 2 Fluorescence titration data of Nile-red solubilization assay to determine the critical aggregation concentration (CAC) of (a) **Chol-$\mathbf{G_1}$** and (b) **Chol-$\mathbf{IG_1}$** in a phosphate buffer solution (PBS, pH = 7.4). The CAC values are calculated by linear extrapolation of the linear regression fitting data.

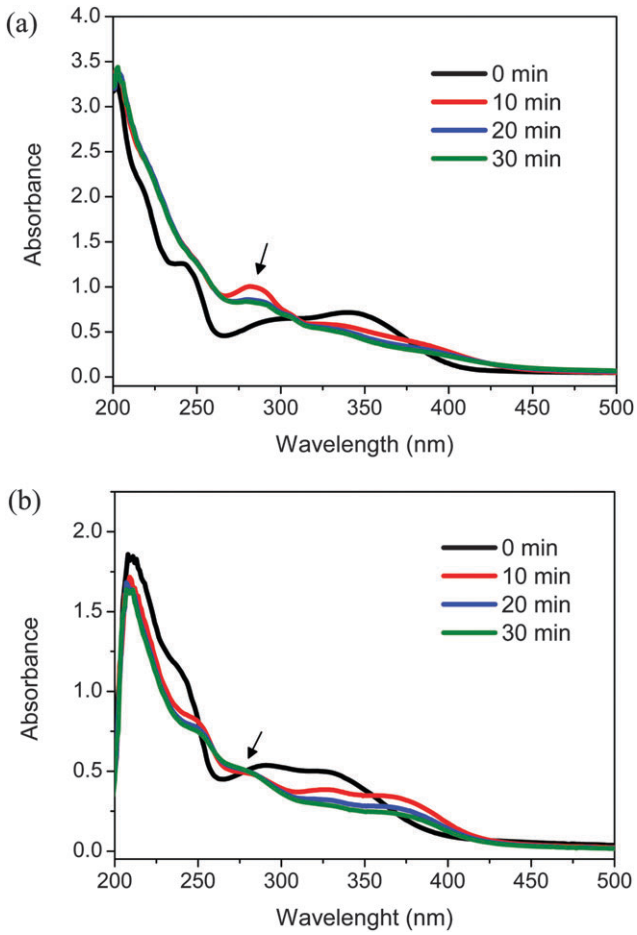

Fig. 3 UV-Vis absorption spectra of (a) **Chol-$\mathbf{G_1}$** and (b) **Chol-$\mathbf{IG_1}$** aqueous solutions under 365 nm light-emitting diode (LED) irradiation. The appearance of an absorption peak at 280 nm indicates successful photolysis of *o*-nitrobenzyl ester. The molar concentration for both dendron solutions is equal to 1×10^{-4} M.

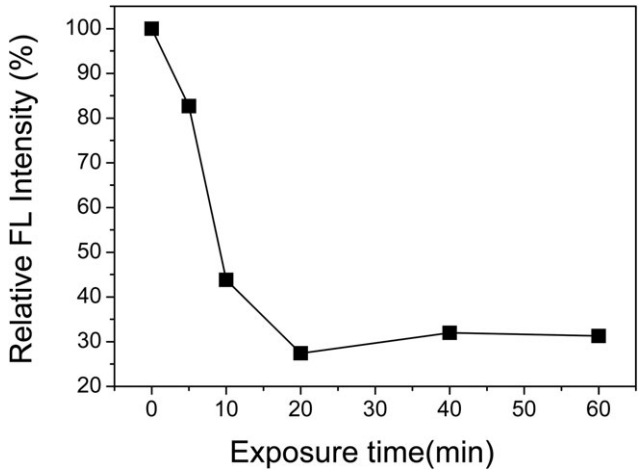

Fig. 4 The relative fluorescence intensity of Nile-red in the presence of **Chol-G$_1$** (100 μM) after 365 nm light irradiation. The sample solutions were exposed to UV light at fixed time intervals, followed by adding the Nile-red probe to analyze the dendron assembly.

absorption peak at 280 nm after light exposure indicates the formation of *o*-nitrosobenzaldehyde (see Fig. S4, ESI†).

Because these amphiphilic dendrons undergo efficient photolytic structural degradation, dissociation of the self-assembled aggregates of the amphiphilic dendrons could also be activated by a UV light trigger. The photoinduced disassembly process of **Chol-G$_1$** aggregates was then analyzed by the Nile-red assay. Notably, the concentration of the dendron solution was kept at 100 μM, which is fairly above the CAC, to ensure the micelle formation. As shown in Fig. 4, the fluorescence intensity of Nile-red dramatically decreases and reaches a plateau after the solution was exposed to UV light for 20 min. This result suggests that the photocleavage of the *o*-NB groups could decompose the amphiphilic structure and thus cause the micelle deformation.

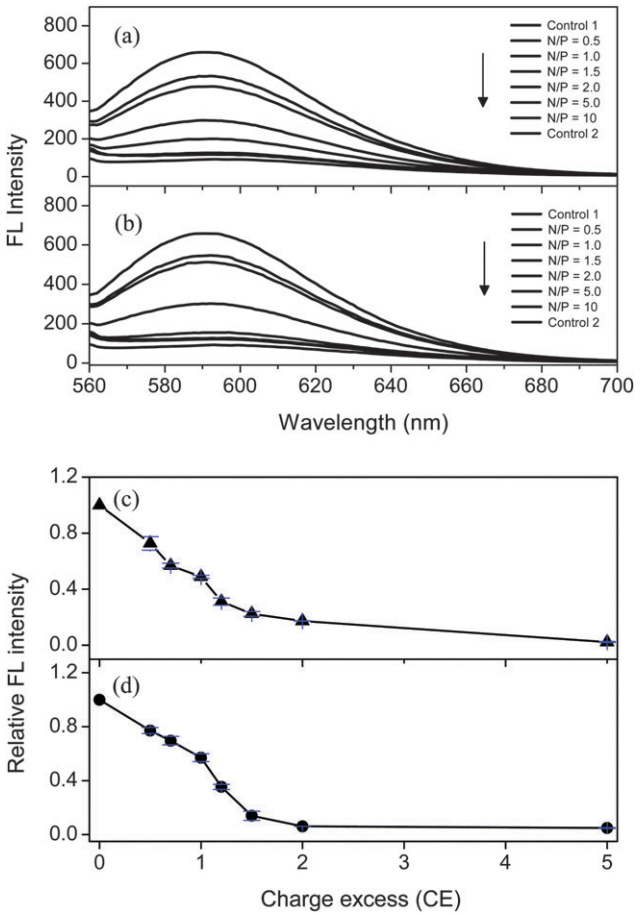

Fig. 5 Fluorescence titration data of ethidum bromide (EtBr) displacement assay for addition of (a) **Chol-G$_1$** and (b) **Chol-IG$_1$** to pEGFP-C1 at increasing nitrogen-to-phosphorous (N/P) ratios. Control 1 corresponds to 1 : 1 binding of EtBr and a DNA base in the absence of dendrons, and control 2 corresponds to the free EtBr in a phosphate buffer solution (PBS, pH = 7.4). The correlation of relative fluorescence intensity of EtBr at 590 nm *versus* the charge excess values of (c) **Chol-G$_1$** and (d) **Chol-IG$_1$** with DNA.

DNA binding and photo-induced releasing

We then used the standard ethidium bromide (EtBr) displacement fluorescence spectroscopic assay to investigate the ''dendriplex'' formation of these dendrons to bind pEGFP-C1 reporter DNA (approximately 4700 base pairs).[33,34] This assay method involves using the competition between the DNA binder and EtBr to determine the concentration at which the DNA binder takes effect. This concentration can be expressed as a charge excess (CE_{50}) value, which reflects the concentration of the DNA binder required for half of the EtBr to be displaced from binding to DNA. This value is also the equivalent of a minimum nitrogen-to-phosphorus (N/P) ratio that is usually used to determine the amount of amine-based binding motifs required for effective DNA condensation through electrostatic interactions between the amine and phosphate groups. Initially, EtBr undergoes a large increase in fluorescence intensity upon intercalation with stacks of nucleic acid base pairs. The fluorometric titration experiments illustrated in Fig. 5a and b reveal the fluorescence quenching of the EtBr/DNA complex in the presence of competing **Chol-G$_1$** and **Chol-IG$_1$**. This fluorescence quenching is due to the competitive displacement of EtBr by the amine-based dendrons.

Moreover, by maintaining the amounts of DNA (0.5 μg) and EtBr (0.7 μg) constant during all fluorometric assays, reduced fluorescence intensity was found to depend on the administered N/P values. As shown in Fig. 5c and d, both amphiphilic dendrons possess similar DNA binding affinity, with calculated CE_{50} values of 0.92 and 0.97 for **Chol-G$_1$** and **Chol-IG$_1$**, respectively, indicating that 50% of the EtBr intercalated in the DNA could be successfully replaced by **Chol-G$_1$** and **Chol-IG$_1$** in phosphate buffer solutions. Accordingly, the minimum N/P ratio for effective DNA complexation is approximately equal to the CE_{50} values. We also performed a control experiment by using both **G$_1$** and **IG$_1$** dendrons as the DNA binder and found no fluorescence reduction at an N/P ratio of 1. This result suggests that the amphiphilic structure containing cholesteryl and PAMAM dendritic counterparts is crucial for DNA

complexation. DNA complexation was further analyzed by recording zeta potential measurements. The pristine pEGFP-C1 possesses a negative surface charge of approximately −54.7 ± 2.6 mV and was neutralized by adding **Chol-G$_1$** at an N/P ratio of 2. The surface potential shifted positively to +0.47 ± 0.1 mV, clearly confirming effective binding between DNA and the vectors above the CE_{50}.

The EtBr assay can also be used to study the UV-light-induced disassembly of the DNA and amphiphilic dendron complexes. We reasoned that as the dendrons degraded under UV light exposure, the DNA should be released and the EtBr is reintercalated into the double helix, thus reactivating its fluorescence. Before the test, two control experiments confirmed that (1) the DNA structure is insensitive to the 365 nm LED because the fluorescence intensity of the EtBr/DNA complex in the absence of amphiphilic dendrons remained at the highest value upon light exposure for 30 min, and (2) the fluorescence intensity remained essentially at the lowest value if the complex solution was maintained in the dark for 24 h in the presence of amphiphilic dendrons at an N/P ratio of 2. This result suggests that the DNA cannot be released from the electrostatic complexes because the amphiphilic dendrons possess an intact structure. The bar chart in Fig. 6 indicates successful DNA release upon UV-light exposure. First, the fluorescence of EtBr at λ_{max} = 590 nm decreases because the EtBr is displaced from the DNA double helix by the presence of **Chol-G$_1$** and **Chol-IG$_1$** at an N/P ratio of 2. After UV light irradiation within 10 min, the clear increase in fluorescence intensity indicates the disassembly of the DNA complexes. UV-Vis analysis demonstrated that both **Chol-G$_1$** and **Chol-IG$_1$** are highly sensitive to UV light, and thus the fluorescence enhancement is apparently due to EtBr reintercalation into DNA resulting from the photoinduced structural degradation of the amphiphilic dendrons that associates with DNA release. DLS measurement also supports the photoinduced dissociation of the DNA complexes. Initially, the dimensions of DNA–**Chol-G$_1$**

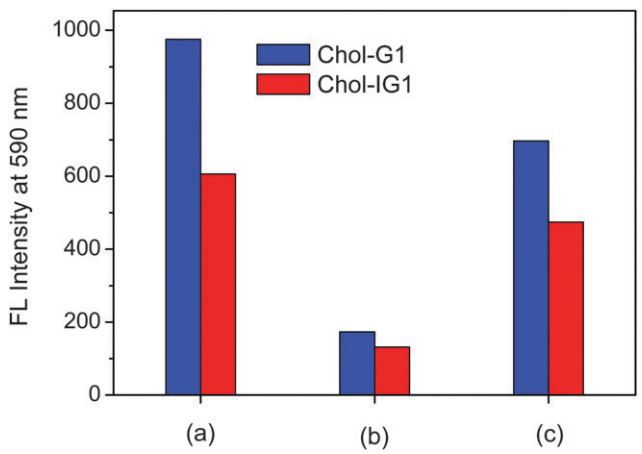

Fig. 6 Fluorescence intensity of EtBr in the presence of (a) pEFGP-C1 and of (b) dendriplexes composed of pEGFP-C1/**Chol-G$_1$** or **Chol-IG$_1$** at N/P = 2. (c) The emission intensity was recovered after 365-nm light irradiation for 10 min, suggesting dendron degradation and EtBr reintercalation into DNA.

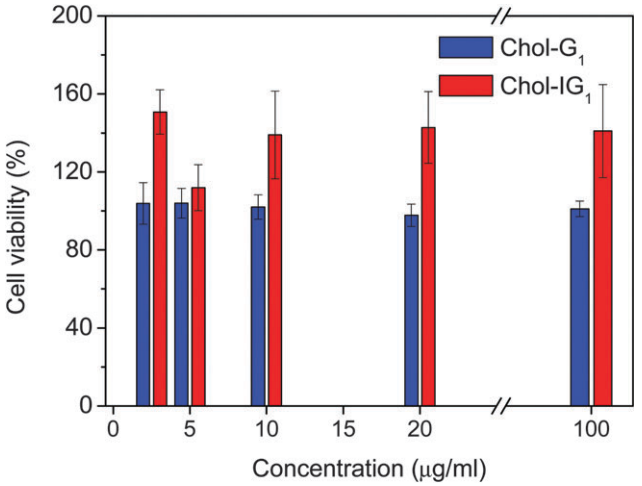

Fig. 7 Smulow–Glikcman (SG) gingival cell viability test in the presence of **Chol-G$_1$** and **Chol-IG$_1$**.

complexes formed in an aqueous buffer solution were approximately 277 ± 57.3 nm; however, after light irradiation, hydrodynamic size distribution was undetectable by the DLS method, suggesting the disappearance of the DNA complexes. Moreover, zeta potential of the complex solution decreases from +0.47 ± 0.1 mV before irradiation to −44.6 ± 1.5 mV after irradiation. This negative shift of surface potential also confirms the phototriggered release of polyanionic DNA into surrounding solutions.

Barnard *et al.* argued that complete dendron degradation is necessary for effective DNA release.[11] However, when bound to DNA, dendron degradation becomes ineffective on a transfection-relevant time scale (hours). We supposed that is because DNA complexation may increase the stability of the dendrons against environmental fluctuation (*e.g.*, the change in pH associated with endosomes). Because a photolabile *o*-NB building block exists in the dendrons, structural breakdown can be effectively triggered using UV light irradiation within several minutes, even in the presence of DNA. This photoinduction strategy enables DNA release on the transfection time scale under an actively triggered route. Moreover, by using water-soluble tetrazolium (WST) salt to assess metabolic cytotoxicity, **Chol-G$_1$** and **Chol-IG$_1$** were found to be nontoxic to the Smulow–Glikcman (SG) gingival cell lines at up to 100 μg mL^{-1} (Fig. 7). The test indicated that high doses of both vectors do not induce a cytotoxic response. The efficiency of gene transfection has been suggested as usually being optimized with increasing N/P ratios, and thus the transfection can be conducted until an approximate N/P value of 50, which is substantially higher than the value for effective DNA binding. *In vivo* gene transfection facilitated by phototriggers toward SG cells by using the photoresponsive amphiphilic dendrons as synthetic vectors is currently under investigation.

Conclusion

In summary, we successfully synthesized photoresponsive amphiphilic PAMAM dendrons bearing photolabile *o*-NB building blocks as DNA carriers. Both amphiphilic dendrons

comprising classical and inverse PAMAM dendritic scaffolds exhibit similar self-assembly behavior in the formation of micelle-like pseudodendrimers in an aqueous solution. On the basis of the bipolar functionality, **Chol-G_1** and **Chol-IG_1** also demonstrate substantial binding affinity with cyclic DNA at low N/P values. Most critically, thus-formed DNA complexes are readily dissociated under UV light irradiation because the *o*-NB group in the dendritic structure undergoes efficient photolytic cleavage, causing effective dendron degradation accompanied by DNA release. This photochemical strategy provides an opportunity to control over the gene binding and releasing in a spatiotemporal manner.

Experimental section

Materials and instruments

All reagents were purchased as high-purity reagent-grade chemicals from either Sigma-Aldrich or Acros and used without further purification. The circular reporter DNA (pEGFP-C1) was a generous gift from Prof. Wen-Wei Chang. The classical poly(amido amine) (PAMAM) dendron (**G_1**) was synthesized *via* a divergent pathway,[28] and the dendron analogue (**IG_1**) was prepared by a solid-phase synthetic method.[27] All organic solvents for organic synthesis were distilled over suitable drying reagents under a N_2 atmosphere before use. ^{1}H (400 MHz) and ^{13}C (75 MHz) NMR spectra were recorded on a Varian Mercury Plus 400 MHz spectrometer at room temperature using $CDCl_3$, DMSO-d_6, methanol-d_4, or D_2O as the solvents. Spectral processing (Fourier transform, peak assignment, and integration) was performed using MestReNova 6.2.1 software. Matrix-assisted laser desorption ionization/time-of-flight mass spectrometry (MALDI-TOF-MS) was performed on a Bruker AutoFlex III TOF/TOF system in positive ion mode using either 2,5-dihydroxybenzoic acid or α-cyano-4-hydroxycinnamic acid as the desorption matrix. The size and zeta potential measurements were recorded on a Horiba SZ-100 nanopartica series instrument using a 532 nm laser as the incident light source. Ultraviolet-visible (UV-Vis) absorption spectra were performed on a Thermo Genesys 10S UV-Vis spectrometer. Fluorescence emission spectra were recorded on a Hitachi F-2500 spectrometer. Photolysis of the ester conjugates were carried out by using light-emitting diodes (LEDs) at 365 nm and an output power of 10 watt.

Synthesis of propargyl-functionalized IG_1

A CH_2Cl_2 solution (2 mL) of dicyclohexylcarbodiimide (DCC, 51 mg, 0.25 mmol) was added dropwise into a CH_2Cl_2 solution (3 mL) of **IG_1** (50 mg, 0.12 mmol), propargylamine (40 μL, 0.62 mmol), and 1-hydroxybenzotriazole (5.1 mg, 10 wt% of DCC) under N_2 at 0 °C. After 15 min, the mixture was then stirred under room temperature overnight. The reaction mixture was cooled to 0 °C to ensure complete precipitation of the byproduct dicyclohexylurea, which is quickly removed by vacuum filtration. After rotatory evaporation to dryness, the crude product was further purified by flash column chromatography (SiO_2, ethyl acetate/hexane 2 : 3) to give propargyl-functionalized **IG_1** as a colorless liquid (36 mg, 66%). ^{1}H-NMR (400 MHz, $CDCl_3$): δ = 4.95 (bs, 2H), 4.04 (dd, J = 5.1, 2.5 Hz, 2H), 3.16 (dd, J = 12.3, 6.2 Hz, 4H), 2.71 (t, J = 6.2 Hz, 2H), 2.46 (t, J = 6.6 Hz, 4H), 2.35 (t, J = 6.2 Hz, 2H), 2.22 (t, J = 2.5 Hz, 1H), 1.60–1.68 (m, 4H), 1.44 (s, 18H). ^{13}C-NMR (75 MHz, $CDCl_3$): δ = 172.4, 156.4, 80.2, 79.5, 71.4, 51.6, 50.9, 38.9, 33.9, 28.9, 28.7, 27.5.

Synthesis of (4-(2-bromoethoxy)-5-methoxy-2-nitrophenyl)methanol 2

4-(Hydroxymethyl)-2-methoxy-5-nitrophenol **1** was synthesized from commercially available vanillin in 4 steps following a modified procedure (see ESI†).[29] To a tetrahydrofuran solution (THF, 25 mL) of **1** (1.35 g, 6.8 mmol), K_2CO_3 (0.88 g, 24 mmol), 18-crown-6 (2.7 g, 37 mmol), and 1,2-dibromoethane (3.5 g, 18 mmol) were added dropwise under N_2. After being stirred at 40 °C for 4 h until the disappearance of compound **1**, the mixture was extracted by ethyl acetate/brine 3 times. The combined organic phase was dried over anhydrous magnesium sulfate, and rotatory evaporation to dryness afforded compound **2** as pale-yellow solids (2.0 g, 96%). ^{1}H-NMR (400 MHz, $CDCl_3$): δ = 7.74 (s, 1H), 7.22 (s, 1H), 4.98 (d, J = 5.8 Hz, 2H), 4.52 (bs, 1H), 4.40 (t, J = 6.4 Hz, 2H), 4.00 (s, 3H), 3.70 (t, J = 6.4 Hz, 2H). ^{13}C-NMR (75 MHz, $CDCl_3$): δ = 154.8, 146.8, 139.7, 133.4, 111.6, 110.3, 68.6, 63.2, 56.7, 28.8.

Synthesis of (4-(2-azidoethoxy)-5-methoxy-2-nitrophenyl)methanol 3

A dimethylformamide solution (DMF, 20 mL) of **2** (0.53 g, 1.7 mmol) and NaN_3 (1.1 g, 17 mmol) was stirred at 90 °C overnight under N_2. The solvent was removed under vacuum, and the mixture was extracted by ethyl acetate/brine 3 times. The combined organic phase was dried over anhydrous magnesium sulfate, and rotatory evaporation to dryness afforded compound **3** as pale-yellow solids (0.32 g, 70%). ^{1}H-NMR (400 MHz, $CDCl_3$): δ = 7.73 (s, 1H), 7.22 (s, 1H), 4.98 (bs, 2H), 4.52 (bs, 1H), 4.25 (t, J = 5.0 Hz, 2H), 4.00 (s, 3H), 3.69 (t, J = 5.0 Hz, 2H). ^{13}C-NMR (75 MHz, $CDCl_3$): δ = 154.8, 146.9, 139.7, 133.4, 111.6, 110.4, 68.6, 63.0, 56.7, 50.2.

Synthesis of cholesterol-functionalized compound 4

A THF solution (10 mL) of **3** (0.10 g, 0.37 mmol), cholesteryl chloroformate (0.2 g, 0.45 mmol), and pyridine (46 μL, 0.57 mmol) was stirred at 40 °C overnight under N_2. The solvent was removed under vacuum, and the crude product was purified by flash column chromatography (SiO_2, ethyl acetate/hexane 1 : 4) to give compound **4** as pale-yellow solids (0.13 g, 52%). ^{1}H-NMR (400 MHz, $CDCl_3$): δ = 7.75 (s, 1H), 7.08 (s, 1H), 5.58 (s, 2H), 5.41 (bs, 1H), 4.50–4.58 (m, 1H), 4.25 (t, J = 4.9 Hz, 2H), 3.98 (s, 3H), 3.70 (t, J = 4.9 Hz, 2H), 2.43 (bs, 2H), 0.85–2.03 (m, 38H), 0.68 (s, 3H). ^{13}C-NMR (75 MHz, $CDCl_3$): δ = 154.5, 154.3, 147.1, 139.5, 139.3, 128.3, 123.4, 110.4, 78.7, 68.6, 66.2, 56.9, 56.7, 56.3, 50.2, 42.5, 39.9, 39.7, 38.2, 37.1, 36.8, 36.4, 36.0, 32.1, 32.0, 28.5, 28.2, 27.9, 24.5, 24.1, 23.1, 22.8, 21.3, 19.5, 18.9, 12.1.

Synthesis of click clusters Chol-G_1 and Chol-IG_1

An anhydrous THF solution of compound **4** (21.0 mg, 30.8 μmol), Boc-protected **G_1** (18 mg, 37.2 μmol) or **IG_1** (17 mg, 38.6

μmol), and CuBr (5.3 mg, 36.9 μmol) was vigorously stirred at room temperature until the complete disappearance of compound **4**. The resulting solution was then extracted with ethyl acetate; the organic phase was washed with aqueous ammonia solution to remove the copper catalyst and then dried over magnesium sulfate. Rotatory evaporation to dryness yields the Boc-protected click clusters quantitatively. For Boc-protected **Chol-G$_1$**, ^{1}H-NMR (400 MHz, $CDCl_3$): δ = 7.78 (s, 1H), 7.70 (s, 1H), 7.08 (s, 1H), 5.56 (s, 2H), 5.40 (bs, 1H), 4.85 (bs, 2H), 4.53 (m, 1H), 4.46 (bs, 2H), 3.97 (s, 3H), 3.40 (bs, 2H), 3.32 (bs, 4H), 3.23 (bs, 4H), 2.74 (bs, 4H), 2.42 (m, 6H), 0.85–2.05 (m, 56H), 0.68 (s, 3H); For Boc-protected **Chol-IG$_1$**, ^{1}H-NMR (400 MHz, $CDCl_3$): δ = 7.86 (s, 1H), 7.69 (s, 1H), 7.07 (s, 1H), 5.56 (s, 2H), 5.39 (bs, 1H), 4.80 (t, J = 5.0 Hz, 2H), 4.50–4.54 (m, 3H), 4.44 (t, J = 5.0 Hz, 2H), 3.97 (s, 3H), 3.08–3.16 (m, 4H), 2.68 (m, 2H), 2.43 (m, 6H), 2.35 (bs, 2H), 0.85–2.03 (m, 60H), 0.68 (s, 3H). Boc-deprotection is readily carried out by acid-promoted hydrolysis. Excess trifluoroacetic acid was added dropwise into an anhydrous CH_2Cl_2 solution of Boc-protected click clusters. The mixture was then stirred under room temperature for 3 days, and the volatiles were removed under reduced pressure. The mixture was rinsed with hexane repetitively to remove excess acid, and then freeze–drying afforded amphiphilic dendrons as yellowish fluffy powders (72% for **Chol-G$_1$**, 63% for **Chol-IG$_1$**). The NMR analysis is shown in the ESI.†

General methods for the photolysis and photorelease

The photolytic reaction was performed by irradiating the sample solutions prepared in a quartz cuvette (1 cm × 1 cm) under a 10 watt LED (365 nm). The distance between the sample and light source was kept at approximately 3 cm, and the exposed solutions were analyzed by either UV-Vis absorption or fluorescence spectroscopy.

Nile-red solubilization assay

A Nile red stock solution (2.5 mM) was prepared in ethanol, and a dendron stock solution was prepared in PBS buffer at various concentrations depending on the starting concentration for the assay. Aliquots of the stock solution were taken and diluted with PBS to the desired concentration in a 1 mL assay volume. Nile red (1 μL) was added and the fluorescence emission was recorded on a spectrofluorometer using an excitation wavelength of 550 nm. Fluorescence intensity was recorded at 635 nm. Experiments were performed in triplicate.

EtBr displacement assay

0.5 mL of pEGFP-C1 solution (1 μg mL^{-1}) and 7 μL of EtBr solution (0.1 mg mL^{-1}) were mixed thoroughly in PBS buffer, followed by adding 8 μL of the dendron solutions to the desired N/P values. EtBr in ultrapure water was measured as the background fluorescence of EtBr, and the solution that only contains pEGFP-C1 and EtBr in a 1 : 1 binding ratio corresponds to the N/P = 0 with maximum emission intensity. The fluorescence emission was recorded on a spectrofluorometer using an excitation of 540 nm, and the emission spectra were recorded from 540 nm to 700 nm. Experiments were performed in triplicate.

WST cell proliferation assay

Prior to cytotoxicity measurement, SG cells were grown in a 96-well plate at a density of 3×10^4 cells per well. After incubation for 24 h, dendron solutions were added into each well to attain the desired concentrations. After incubation at 37 °C for 48 h, a solution of 2-(4-iodophenyl)-3-(4-nitrophenyl)-5-(2,4-disulfophenyl)-2*H*-tetrazolium salt (WST-1) as 10 μL per well was added and the mixture was incubated at 37 °C for another 3 h. The viability of the cells was determined by visible absorbance at 440 nm after subtracting the reference absorbance at 650 nm with an ELISA microplate reader (EZ Read 400, Biochrom Ltd, Cambridge, UK). Four independent experiments were performed, and each experiment was done in triplicate.

Acknowledgements

The authors would like to thank Chung Shan Medical University and Ministry of Science and Technology (MOST) of Taiwan, for financially supporting this research (MOST103-2113-M-040-003). The authors are also grateful to Prof. Hsieh-Chih Tsai for support with size and zeta potential measurements and to Prof. Wen-Wei Chang for support with the cytotoxicity test.

References

1 P. Posocco, S. Pricl, S. Jones, A. Barnard and D. K. Smith, *Chem. Sci.*, 2010, **1**, 393–404.
2 S. P. Jones, N. P. Gabrielson, C.-H. Wong, H.-F. Chow, D. W. Pack, P. Posocco, M. Fermeglia, S. Pricl and D. K. Smith, *Mol. Pharmaceutics*, 2011, **8**, 416–429.
3 D. J. Welsh and D. K. Smith, *Org. Biomol. Chem.*, 2011, **9**, 4795–4801.
4 A. Barnard and D. K. Smith, *Angew. Chem., Int. Ed.*, 2012, **51**, 6572–6581.
5 A. Barnard, P. Posocco, M. Fermeglia, A. Tschiche, M. Calderon, S. Pricl and D. K. Smith, *Org. Biomol. Chem.*, 2014, **12**, 446–455.
6 B. N. S. Thota, H. v. Berlepsch, C. Bottcher and R. Haag, *Chem. Commun.*, 2015, **51**, 8648–8651.
7 K. Kono, R. Ikeda, K. Tsukamoto, E. Yuba, C. Kojima and A. Harada, *Bioconjugate Chem.*, 2012, **23**, 871–879.
8 T. Yu, X. Liu, A.-L. Bolcato-Bellemin, Y. Wang, C. Liu, P. Erbacher, F. Qu, P. Rocchi, J.-P. Behr and L. Peng, *Angew. Chem., Int. Ed.*, 2012, **51**, 8478–8484.
9 E. Yuba, Y. Nakajima, K. Tsukamoto, S. Iwashita, C. Kojima, A. Harada and K. Kono, *J. Controlled Release*, 2012, **160**, 552–560.
10 X. Liu, C. Liu, J. Zhou, C. Chen, F. Qu, J. J. Rossi, P. Rocchi and L. Peng, *Nanoscale*, 2015, **7**, 3867–3875.
11 A. Barnard, P. Posocco, S. Pricl, M. Calderon, R. Haag, M. E. Hwang, V. W. T. Shum, D. W. Pack and D. K. Smith, *J. Am. Chem. Soc.*, 2011, **133**, 20288–20300.
12 B. Draghici and M. A. Ilies, *J. Med. Chem.*, 2015, **58**, 4091–4130.
13 S. Bhatia and R. Haag, in *Targeted Drug Delivery: Concepts and Design*, ed. P. V. Devarajan and S. Jain, Springer International Publishing, 2015, pp. 543–569.

14 M. R. Molla, P. Rangadurai, G. M. Pavan and S. Thayumanavan, *Nanoscale*, 2015, **7**, 3817–3837.
15 R.-S. Lee, S.-W. Wang, Y.-C. Li and J.-Y. Fang, *RSC Adv.*, 2015, **5**, 497–512.
16 Z. Jiang, H. Li, Y. You, X. Wu, S. Shao and Q. Gu, *J. Biomed. Mater. Res., Part A*, 2015, **103**, 65–70.
17 S. Shah, P. K. Sasmal and K.-B. Lee, *J. Mater. Chem. B*, 2014, **2**, 7685–7693.
18 Q. Jin, Y. Wang, T. Cai, H. Wang and J. Ji, *Polymer*, 2014, **55**, 4641–4650.
19 Q. Huang, T. Liu, C. Bao, Q. Lin, M. Ma and L. Zhu, *J. Mater. Chem. B*, 2014, **2**, 3333–3339.
20 L. L. Fedoryshin, A. J. Tavares, E. Petryayeva, S. Doughan and U. J. Krull, *ACS Appl. Mater. Interfaces*, 2014, **6**, 13600–13606.
21 H. Zhao, E. S. Sterner, E. B. Coughlin and P. Theato, *Macromolecules*, 2012, **45**, 1723–1736.
22 S. K. Choi, M. Verma, J. Silpe, R. E. Moody, K. Tang, J. J. Hanson and J. R. Baker, *Bioorg. Med. Chem.*, 2012, **20**, 1281–1290.
23 S. K. Choi, T. Thomas, M.-H. Li, A. Kotlyar, A. Desai and J. R. Baker, *Chem. Commun.*, 2010, **46**, 2632–2634.
24 C. Bao, L. Zhu, Q. Lin and H. Tian, *Adv. Mater.*, 2015, **27**, 1647–1662.
25 M. S. Kim and S. L. Diamond, *Bioorg. Med. Chem. Lett.*, 2006, **16**, 4007–4010.
26 J. Liu, C. Detrembleur, S. Mornet, C. Jerome and E. Duguet, *J. Mater. Chem. B*, 2015, **3**, 6117–6147.
27 A. Y.-T. Huang, C.-H. Tsai, H.-Y. Chen, H.-T. Chen, C.-Y. Lu, Y.-T. Lin and C.-L. Kao, *Chem. Commun.*, 2013, **49**, 5784–5786.
28 C.-H. Hung, W.-W. Chang, S.-C. Liu, S.-J. Wu, C.-C. Chu, Y.-J. Tsai and T. Imae, *J. Biomed. Mater. Res., Part A*, 2015, **103**, 1595–1604.
29 H. Mizuta, S. Watanabe, Y. Sakurai, K. Nishiyama, T. Furuta, Y. Kobayashi and M. Iwamura, *Bioorg. Med. Chem.*, 2002, **10**, 675–683.
30 D. A. Tomalia, *New J. Chem.*, 2012, **36**, 264–281.
31 P. Greenspan, E. P. Mayer and S. D. Fowler, *J. Cell Biol.*, 1985, **100**, 965–973.
32 J. E. T. Corrie, A. Barth, V. R. N. Munasinghe, D. R. Trentham and M. C. Hutter, *J. Am. Chem. Soc.*, 2003, **125**, 8546–8554.
33 W. Fischer, M. A. Quadir, A. Barnard, D. K. Smith and R. Haag, *Macromol. Biosci.*, 2011, **11**, 1736–1746.
34 C. Ramaswamy, T. Sakthivel, A. F. Wilderspin and A. T. Florence, *Int. J. Pharm.*, 2003, **254**, 17–21.

Supporting Information

Photodegradable Self-Assembling PAMAM Dendrons for Gene Delivery Involving Dendriplexes Formation and Phototriggered Circular DNA Release

Yu-Sen Lai,[a] Chai-Lin Kao,[b] Ya-Pei Chen,[a] Chia-Chia Fang,[a] Chao-Chin Hu [a] and Chih-Chien Chu[a,c]

[a]Department of Medical Applied Chemistry, Chung Shan Medical University, Taichung 40201, Taiwan
[b]Department of Medical and Applied Chemistry, Kaohsiung Medical University, Kaohsiung 80708, Taiwan
[c]Department of Medical Education, Chung Shan Medical University Hospital, Taichung 40201, Taiwan

Synthesis of compound *1*

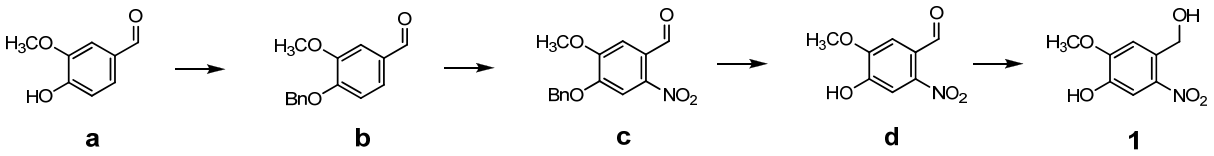

4-(benzyloxy)-3-methoxybenzaldehyde *b*

To a dimethylsulfoxide solution (DMSO, 60 mL) of vanillin ***a*** (8.50 g, 55.8 mmol) and K_2CO_3 (3.86 g, 27.9 mmol), benzyl chloride (12.8 g, 101 mmol) was added dropwise under N_2. After stirred at 90 °C for 15 h until the disappearance of vanillin, the mixture was cooled to room temperature and then poured into water (100 mL). The organic phase was extracted by ethyl acetate, and rotatory evaporation to dryness afforded the crude product. Recrystallization from ethanol yields compound ***b*** as white solids (12.3 g, 91%). ^{1}H-NMR (400 MHz, $CDCl_3$): δ = 9.83 (s, 1H), 7.30-7.45 (m, 7H), 6.99 (d, *J* = 8.2 Hz, 1H), 5.25 (s, 2H), 3.95 (s, 3H). ^{13}C-NMR (75 MHz, $CDCl_3$): δ = 191.1, 153.8, 150.3, 136.2, 130.5, 128.9, 128.4, 127.4, 126.8, 112.6, 109.6, 71.1, 56.3.

4-(benzyloxy)-5-methoxy-2-nitrobenzaldehyde *c*

Compound ***b*** (5.67 g, 23.4 mmol) was dissvoled in acetic acid (70 mL), followed by adding 65% of nitric acid (10.5 mL) dropwisely under ice bath. The reaction mixture was then stirred

at room temperature for overnigh. The mixture was poured into crused ice, and the nitrified product was extracted by ethyl acetate for 3 times. Combined organic phase was dried over anhydrous magnesium sulfate, and rotatory evaporation to dryness afforded crude compound. Flash column chromatography (SiO_2, ethyl acetate/hexane 3:7) yields compound ***c*** as yellow solids as yellow solids (5.11 g, 76%). ^{1}H-NMR (400 MHz, $CDCl_3$): δ = 10.44 (s, 1H), 7.67 (s, 1H), 7.30-7.47 (m, 6H), 5.27 (s, 2H), 4.02 (s, 3H).

4-hydroxy-5-methoxy-2-nitrobenzaldehyde *d*

A trifluoroacetic acid solution (TFA, 25 mL) of compound ***c*** (2.29 g, 7.97 mmol) was stirred at room temperature for overnight under N_2. The volatile was removed under vacuum, and the crude product was rinsed with hexane until complete removal of TFA. Compound ***d*** was then obtained as pale-yellow solids (1.26 g, 80%). ^{1}H-NMR (400 MHz, DMSO-d_6): δ = 10.40 (s, 1H), 7.68 (s, 1H), 7.46 (s, 1H), 4.07 (s, 3H). ^{13}C-NMR (75 MHz, DMSO-d_6): δ = 187.9, 151.9, 150.5, 143.5, 124.1, 111.2, 110.0, 55.8.

4-(hydroxymethyl)-2-methoxy-5-nitrophenol *1*

A ethanol solution (30 mL) of compound ***d*** (2.92 g, 14.8 mmol) was slowly added by $NaBH_4$ (2.80 g, 74.0 mmol), and then the reaction mixture was stirred at room temperature until the disappearance of compound ***d***. The reaction was quenched by water (5 mL) under ice bath, and the crude product was extracted by ethyl acetate/brine for 3 times. Combined organic phase was dried over anhydrous magnesium sulfate, and rotatory evaporation to dryness afforded compound ***1*** as pale-yellow solids (2.86 g, 97%). ^{1}H-NMR (400 MHz, CD_3OD): δ = 7.59 (s, 1H), 7.35 (s, 1H), 4.92 (s, 2H), 3.98 (s, 3H). ^{13}C-NMR (75 MHz, CD_3OD): δ = 152.9, 145.5, 139.5, 131.8, 111.5, 109.7, 61.1, 55.5.

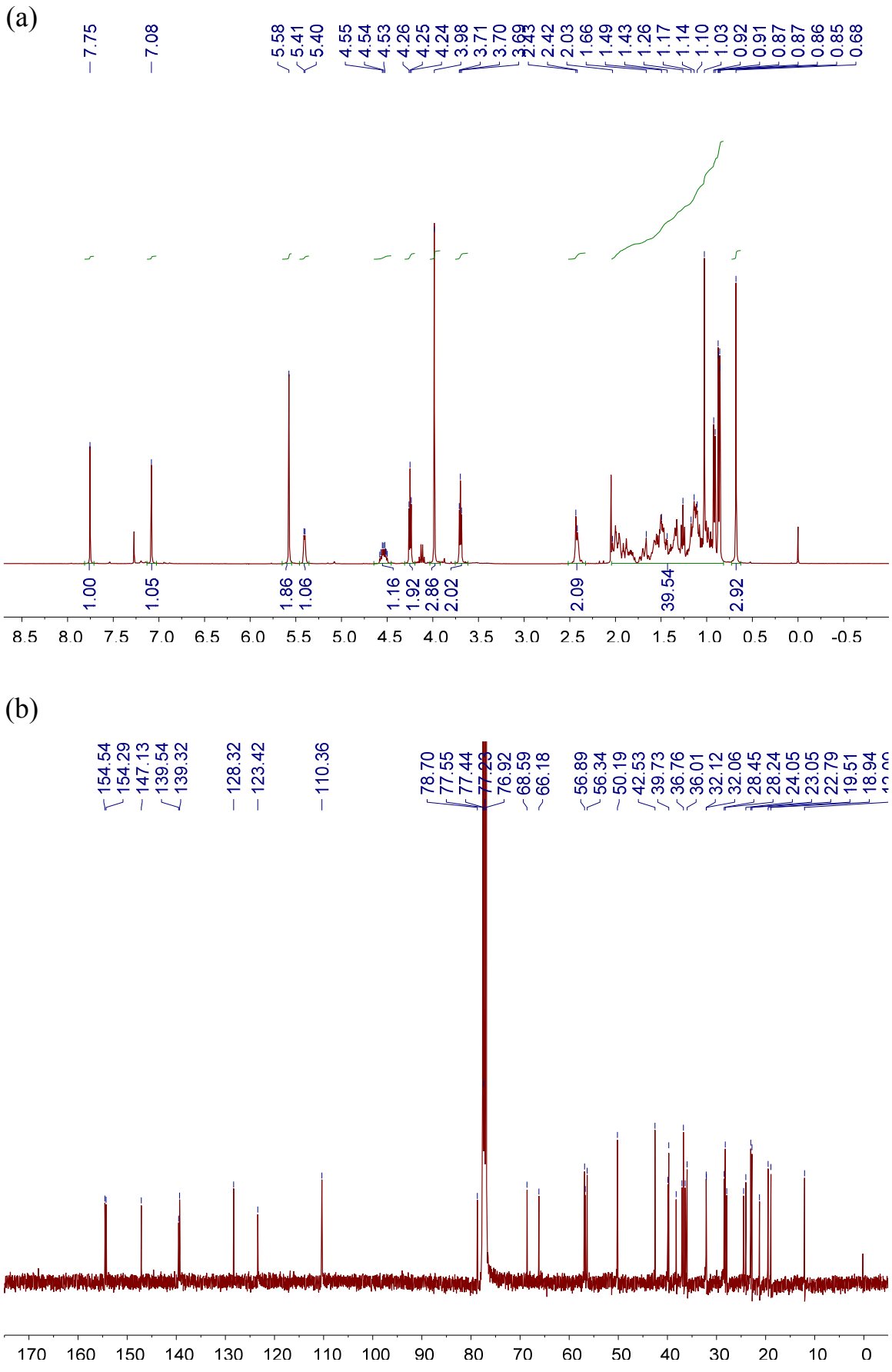

Figure S1. (a) ^{1}H and (b) ^{13}C-NMR spectra of compound ***4*** in $CDCl_3$ at 25 ºC.

Chol-G_1

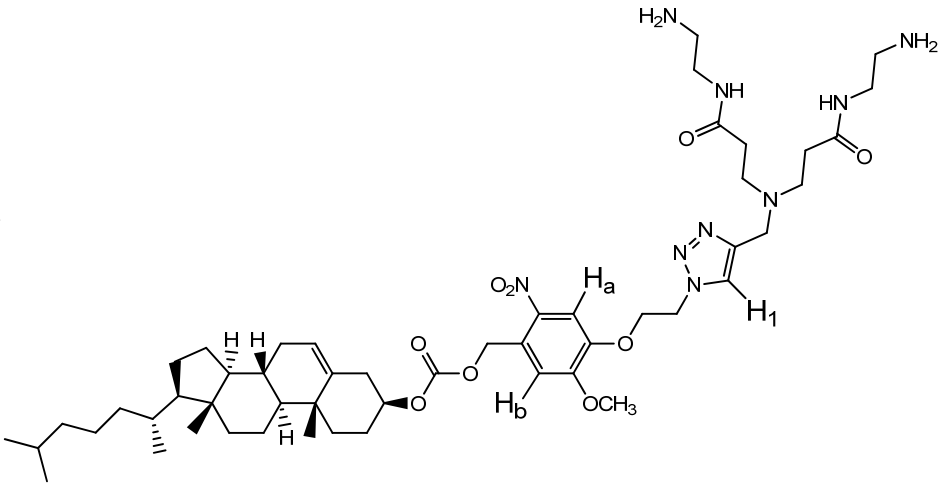

Chol-IG_1

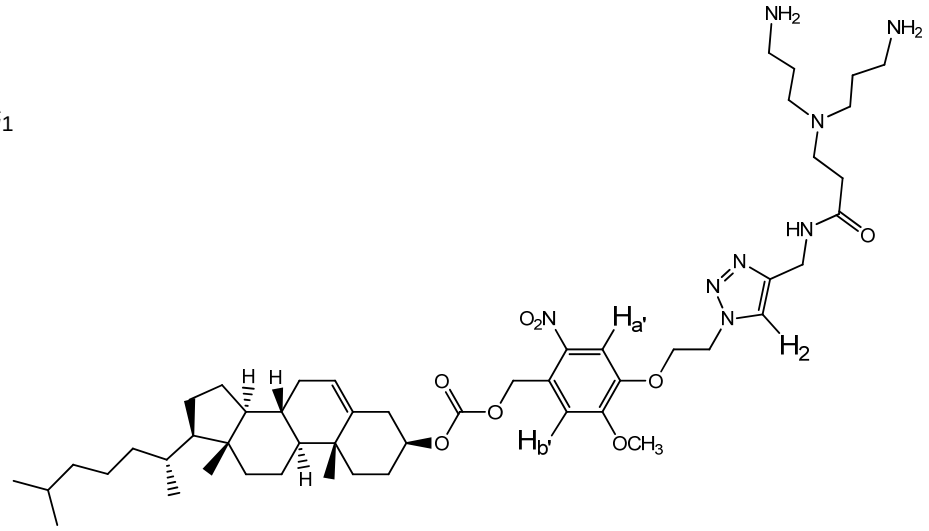

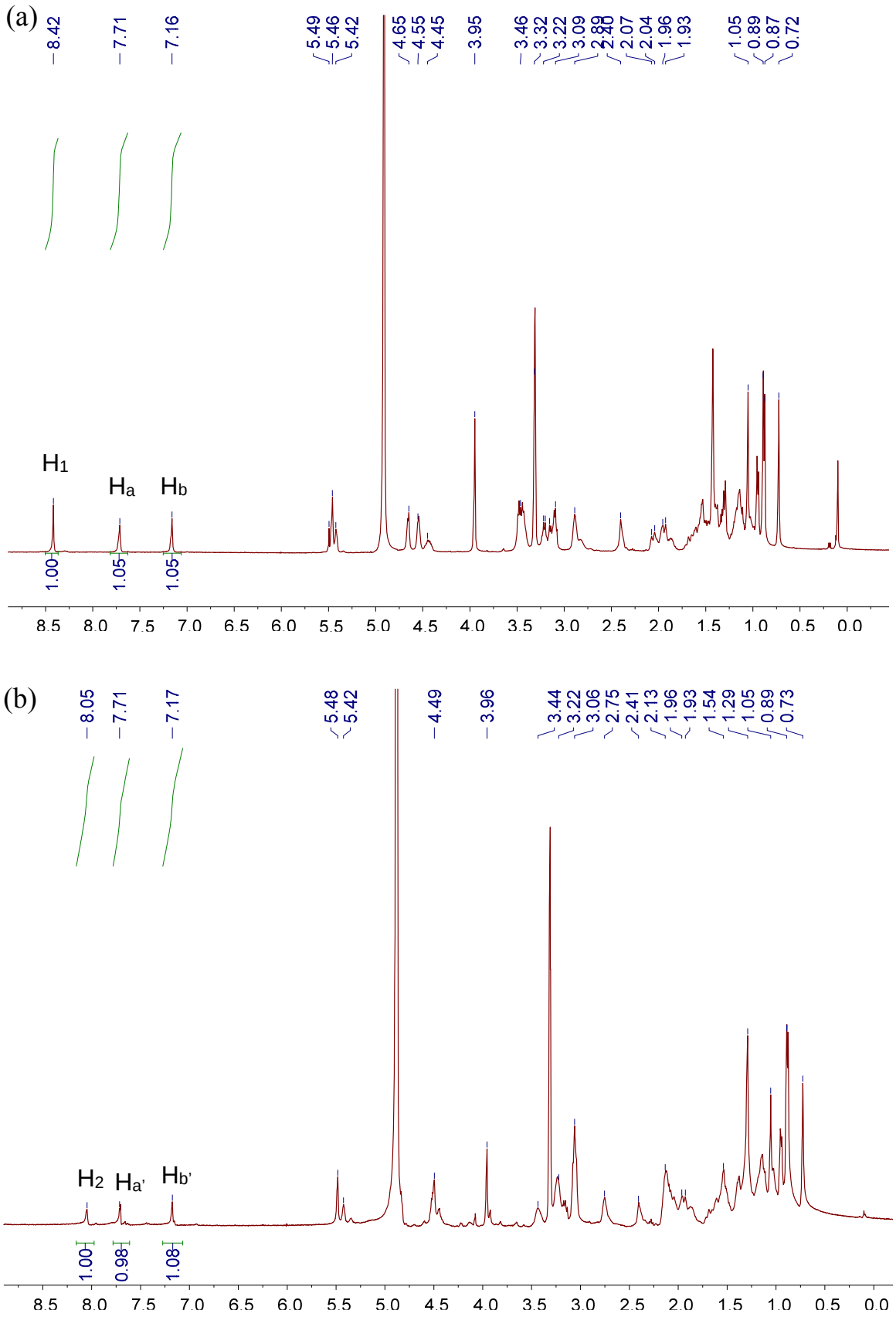

Figure S2. ^{1}H-NMR spectra of (a) **Chol-*G*$_1$** and (b) **Chol-I*G*$_1$** in CD_3OD at 25 °C. The assigned peaks denote to the protons on the triazole (H_1, H_2) and *o*-nitrobenzyl rings (H_a, H_b, $H_{a'}$, and $H_{b'}$), which indicates successful click reaction.

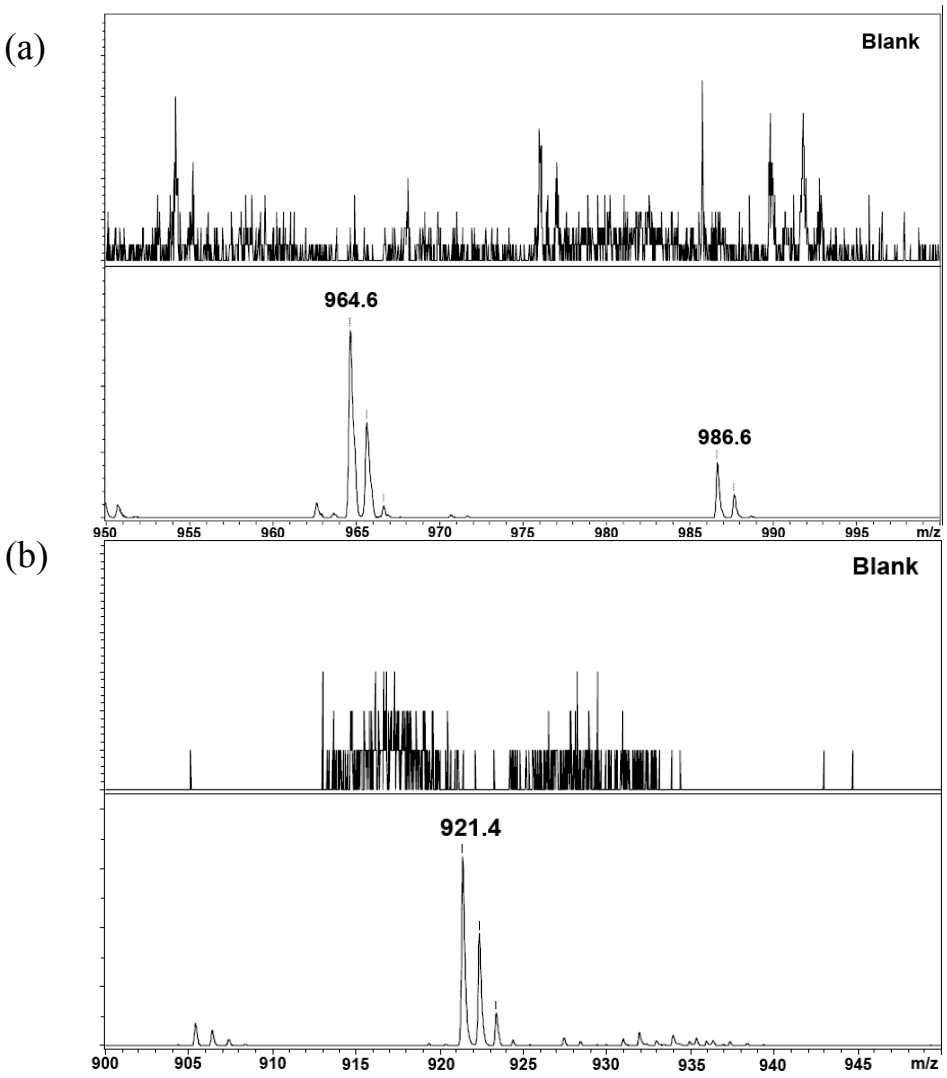

Figure S3. MALDI-TOF-MS spectra of (a) **Chol-G$_1$** and (b) **Chol-IG$_1$** as the protonated (MH^+) and sodium adducts (MNa^+). M denotes to the molecular mass.

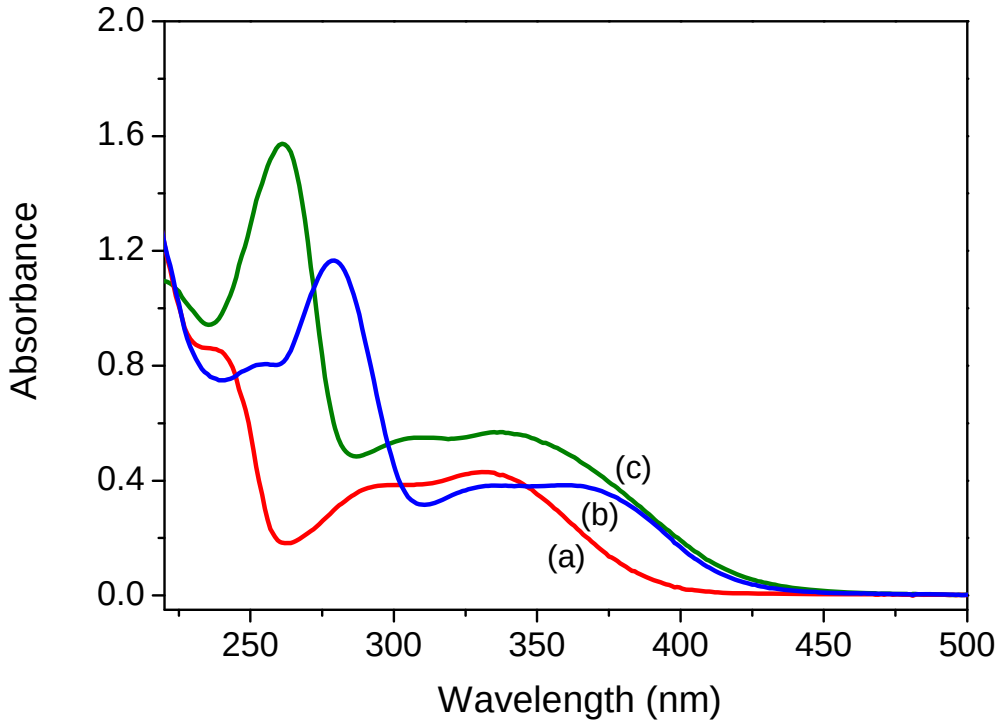

Figure S4. UV-Vis absorption spectra of **Chol-G_1** methanolic solution (a) before and (b) after 365-nm light irradiation and of (c) 4-hydroxy-5-methoxy-2-nitrobenzaldehyde ***d.*** The peak at 280 nm and red-shifted absopriton pattern of (b) is close to the absorption profile of (c), suggesting a successful photolysis reaction.

(a)

Cumulant Operations
Z-Average : 114.9 nm
PI : 0.201
Molecular weight measurement
Molecular weight : ---
Mark-Houwink-Sakurada parameters : ---

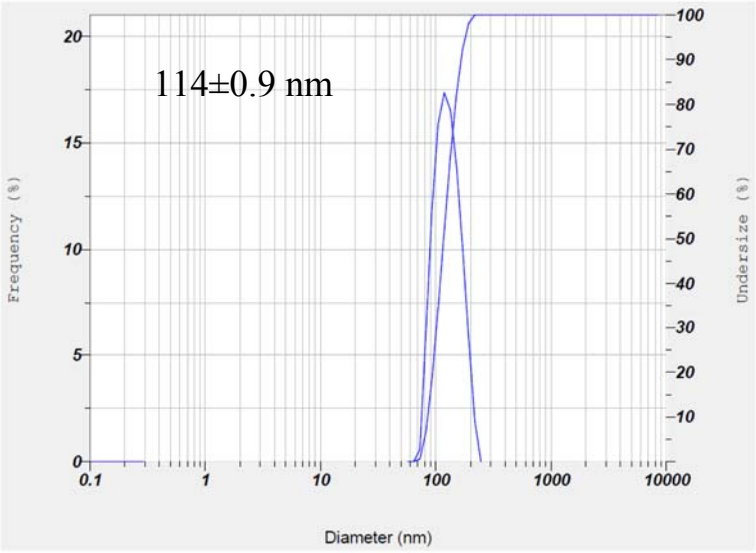

Cumulant Operations
Z-Average : 131.0 nm
PI : 0.189
Molecular weight measurement
Molecular weight : ---
Mark-Houwink-Sakurada parameters : ---

(b)

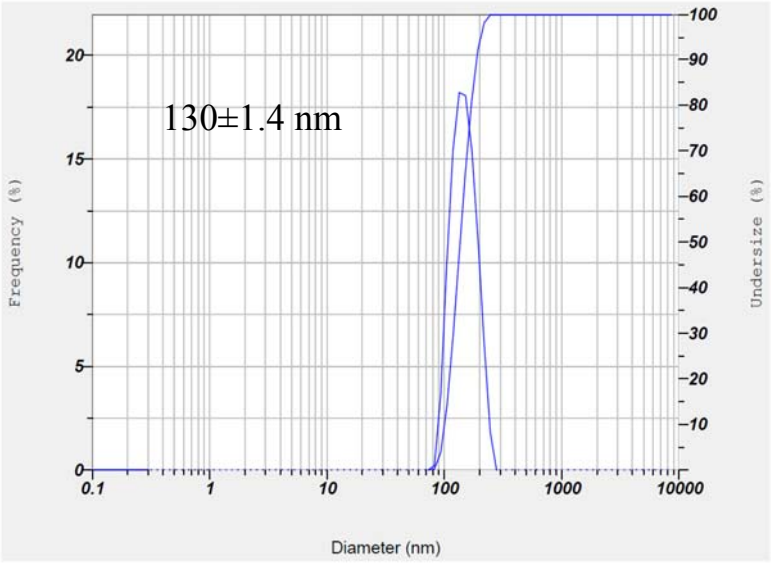

Figure S5. Particle size analysis for the phosphate buffer solutions (PBS, pH = 7.4) of (a) **Chol-G_1** and (b) **Chol-IG_1** (100 μM). The z-averaged size distribution was expressed as mean±standard deviation of three measurements.

Cumulant Operations

Z-Average	: 251.5 nm
PI	: 0.793

Molecular weight measurement

Molecular weight	: ---
Mark-Houwink-Sakurada parameters	: ---

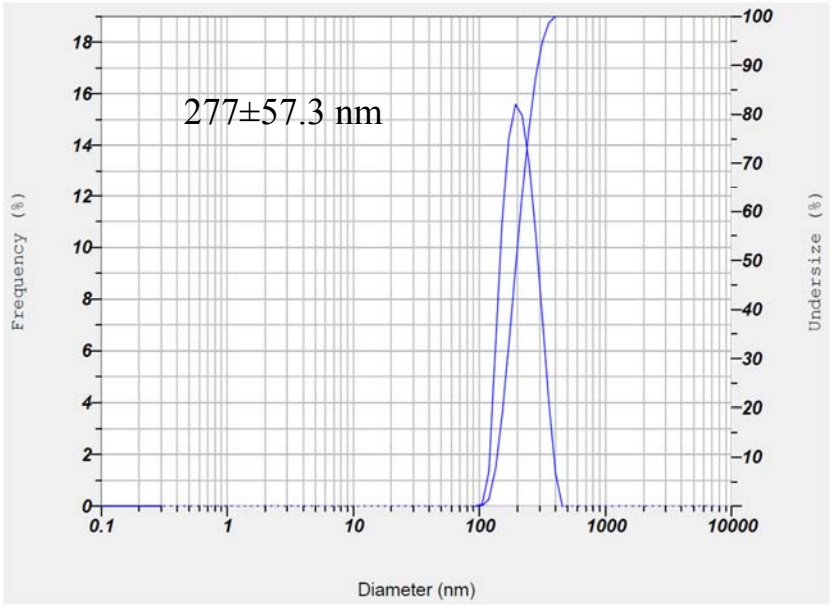

Figure S6. Particle size analysis for the DNA-**Chol-G_1** complexes formed in a phosphate buffer solution at N/P = 2. The z-averaged size distribution was expressed as mean±standard deviation of three measurements.

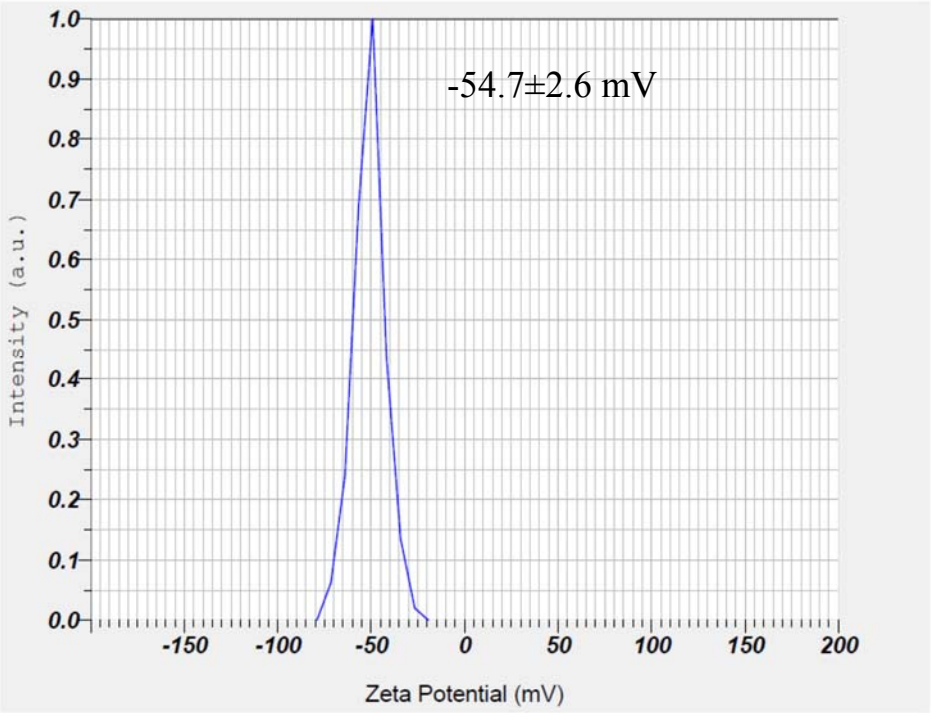

Figure S7. Zeta potential analysis for plasmid DNA (pEGFP-C1) in aqueous solution. The data was expressed as as mean±standard deviation of three measurements.

(a)

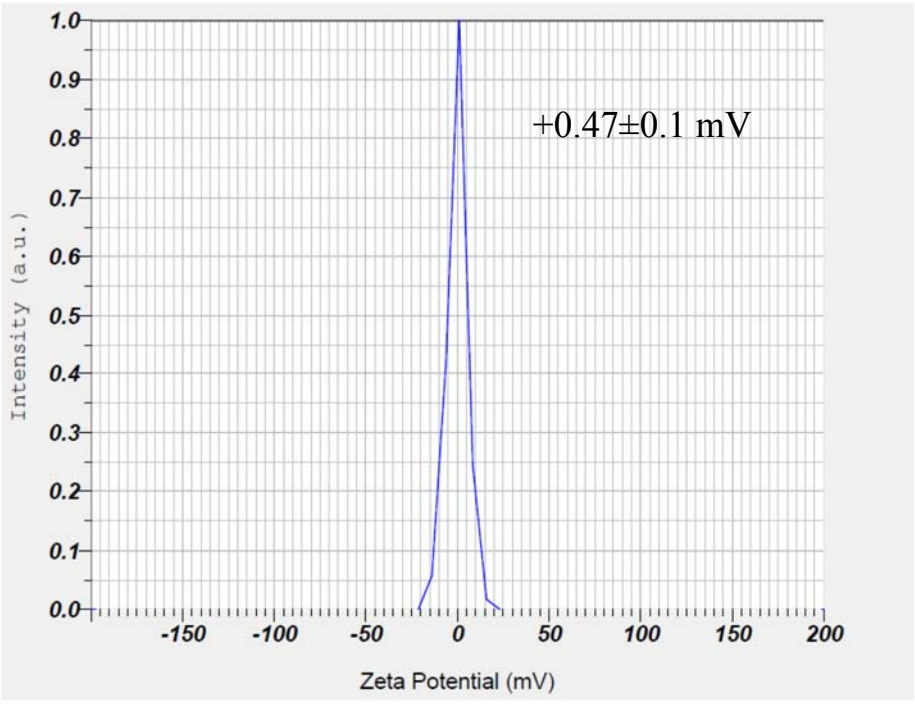

(b)

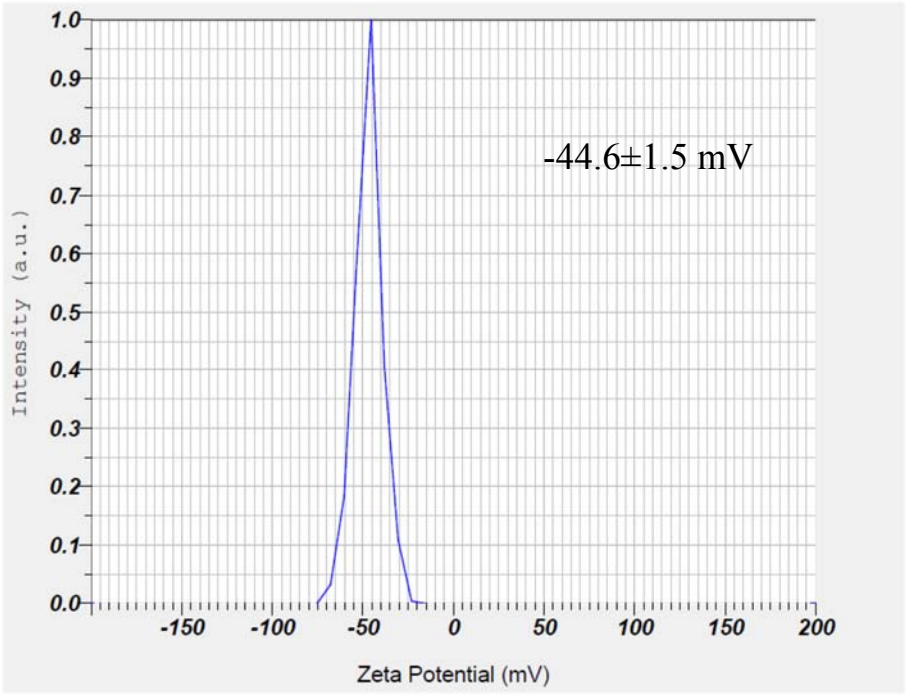

Figure S8. Zeta potential analysis for DNA-**Chol-G_1** complexes formed in a phosphate buffer solution at N/P = 2 (a) before and (b) after 365-nm light irradiation. The data was expressed as as mean±standard deviation of three measurements.

科技部補助計畫衍生研發成果推廣資料表

日期:2016/01/08

科技部補助計畫	計畫名稱: 光敏感型兩性樹枝狀分子的合成、自組裝行為、與其在生醫上的應用
	計畫主持人: 朱智謙
	計畫編號: 103-2113-M-040-003- 學門領域: 有機化學

無研發成果推廣資料

103年度專題研究計畫研究成果彙整表

計畫主持人：朱智謙	**計畫編號：**103-2113-M-040-003-
計畫名稱：光敏感型兩性樹枝狀分子的合成、自組裝行為、與其在生醫上的應用	

成果項目			量化			單位	備註（質化說明：如數個計畫共同成果、成果列為該期刊之封面故事...等）
			實際已達成數（被接受或已發表）	預期總達成數（含實際已達成數）	本計畫實際貢獻百分比		
國內	論文著作	期刊論文	0	0	100%	篇	
		研究報告/技術報告	0	0	100%		
		研討會論文	3	3	100%		
		專書	0	0	100%	章/本	
	專利	申請中件數	0	0	100%	件	
		已獲得件數	0	0	100%		
	技術移轉	件數	0	0	100%	件	
		權利金	0	0	100%	千元	
	參與計畫人力（本國籍）	碩士生	2	2	100%	人次	
		博士生	0	0	100%		
		博士後研究員	0	0	100%		
		專任助理	0	0	100%		
國外	論文著作	期刊論文	2	3	67%	篇	
		研究報告/技術報告	0	0	100%		
		研討會論文	1	1	100%		
		專書	0	0	100%	章/本	
	專利	申請中件數	0	0	100%	件	
		已獲得件數	0	0	100%		
	技術移轉	件數	0	0	100%	件	
		權利金	0	0	100%	千元	
	參與計畫人力（外國籍）	碩士生	0	0	100%	人次	
		博士生	0	0	100%		
		博士後研究員	0	0	100%		
		專任助理	0	0	100%		

其他成果（無法以量化表達之成果如辦理學術活動、獲得獎項、重要國際合作、研究成果國際影響力及其他協助產業技術發展之具體效益事項等，請以文字敘述填列。）	無。

	成果項目	量化	名稱或內容性質簡述
科教處計畫加填項目	測驗工具(含質性與量性)	0	
	課程/模組	0	
	電腦及網路系統或工具	0	
	教材	0	
	舉辦之活動/競賽	0	
	研討會/工作坊	0	
	電子報、網站	0	
	計畫成果推廣之參與（閱聽）人數	0	

科技部補助專題研究計畫成果報告自評表

請就研究內容與原計畫相符程度、達成預期目標情況、研究成果之學術或應用價值（簡要敘述成果所代表之意義、價值、影響或進一步發展之可能性）、是否適合在學術期刊發表或申請專利、主要發現或其他有關價值等，作一綜合評估。

1. 請就研究內容與原計畫相符程度、達成預期目標情況作一綜合評估
   ■達成目標
   □未達成目標（請說明，以100字為限）
   　□實驗失敗
   　□因故實驗中斷
   　□其他原因
   說明：

2. 研究成果在學術期刊發表或申請專利等情形：
   論文：□已發表 □未發表之文稿 ■撰寫中 □無
   專利：□已獲得 □申請中 ■無
   技轉：□已技轉 □洽談中 ■無
   其他：（以100字為限）

3. 請依學術成就、技術創新、社會影響等方面，評估研究成果之學術或應用價值（簡要敘述成果所代表之意義、價值、影響或進一步發展之可能性）（以500字為限）
   本計劃目標為兩親性樹枝狀分子的合成製備、DNA 複合體的型態分析與物理化學性質分析、以及初步基因轉染效率的探討。自評目前的研究成果符合原先設定之目標。我們利用高效率的合成方法合成出一系列兩性基因載體，
   經過初步測試後證明此材料具有不錯的DNA 結合能力與光控釋放能力。我們也嘗試利用Langmuir介面單分子層分析法來研究分子自組裝行為與光敏感現象。目前正在積極嘗試in vivo 細胞生物相關研究。基於這些發現，除了能夠發表相關的學術論文之外，也可以思考與臨床醫學治療結合的可能性。